SUPPLEMENTARY MATERIALS FOR

Reference-quality bat genomes illuminate adaptations to viral tolerance and disease resistance

Ariadna E. Morales [1,2,3,*], Yue Dong [4,5,*], Thomas Brown [6,7], Kaushal Baid [8], Dimitrios - Georgios Kontopoulos [1,2,3], Victoria Gonzalez [8,9], Zixia Huang [10], Alexis-Walid Ahmed [1,2,3], Leon Hilgers [1,2,3], Sylke Winkler [6,7], Graham Hughes [10], Xiaomeng Li [5,4], Bogdan M. Kirilenko [1,2,3], Paolo Devanna [11], Tanya M. Lama [12,], Yomiran Nissan [13,14], Martin Pippel [6,7], Liliana M. Dávalos [12,15], Sonja C. Vernes [11,16], Sebastien J. Puechmaille [17,18], Stephen J. Rossiter [19], Yovel Yossi [14,15], Joseph B. Prescott [20], Andreas Kurth [20], David A. Ray [21], Burton K. Lim [22], Eugene Myers [6,7], Emma C. Teeling [10], Arinjay Banerjee [8,9,23,24,25], Aaron T. Irving [26,5,4,#], Michael Hiller [1,2,3,#]

The Supplement contains:

- Supplementary Figures 1 – 34

Supplementary Tables 1 - 18 are provided as sheets in a separate Excel file.

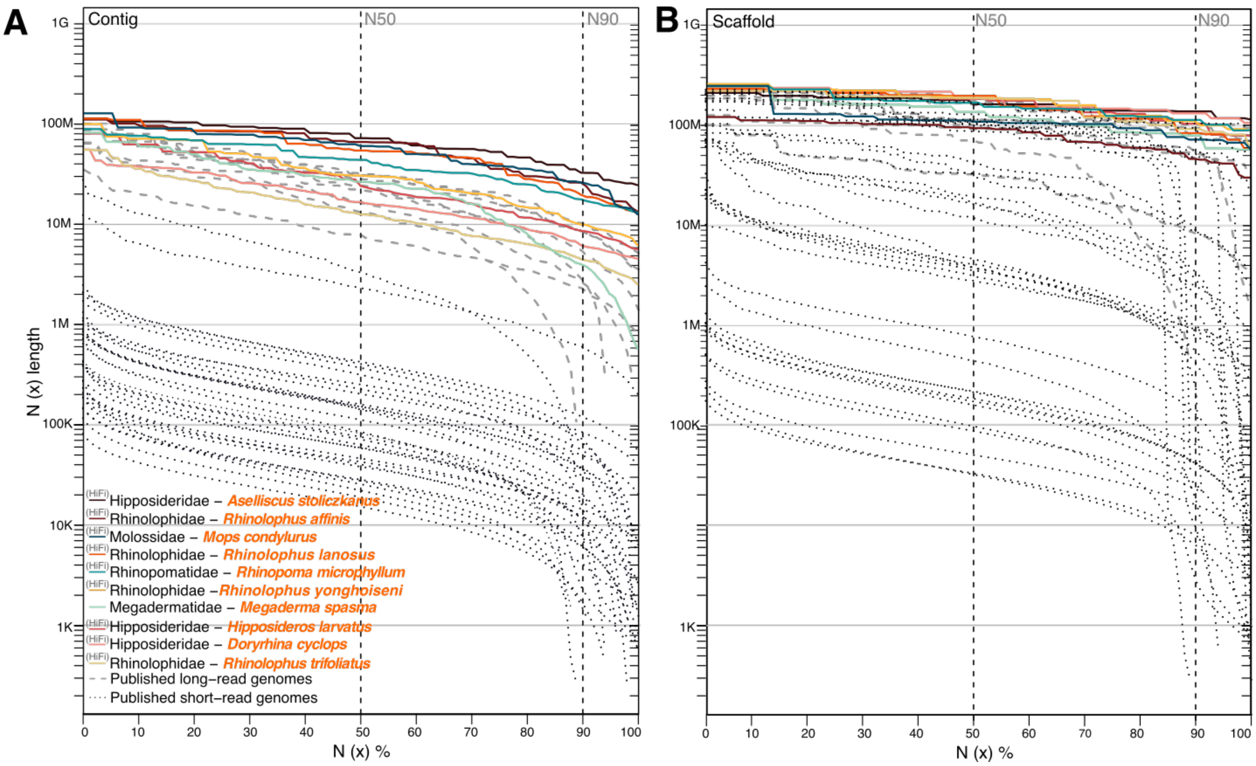

Supplementary Figure 1. Assembly contiguity comparison across 50 bat genomes.
This figure expands on Figure 1C and D by showing 30 short-read based genome assemblies (black dotted lines) of bats that we omitted from the main text figure to improve clarity. The 10 newly-generated (colored solid lines) and 10 published (grey dashed lines) long-read based assemblies are reproduced for comparability. N(x) % graphs show contig (A) and scaffold (B) sizes (y-axis), in which x percent of the assembly consists of contigs and scaffolds of at least that size. Short-read based assemblies consistently have shorter contigs, and also tend to have shorter scaffolds.

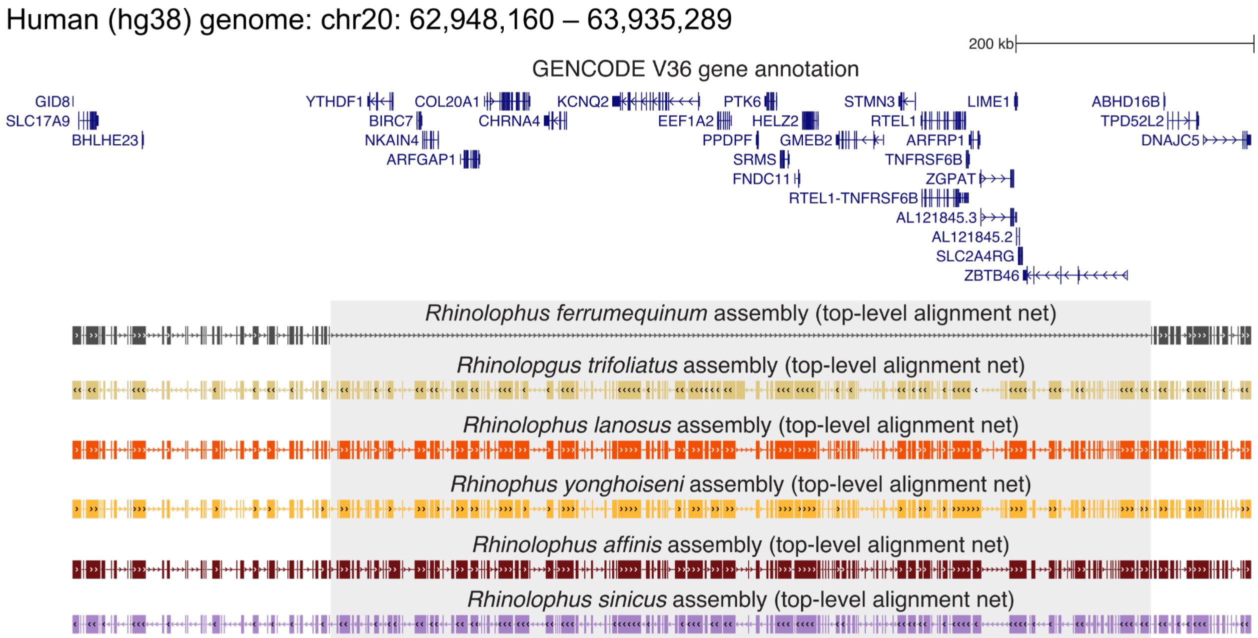

Supplementary Figure 2. PacBio HiFi sequencing improves genome assembly contiguity. UCSC genome browser screenshot showing a 700 kb locus of the human chr20 and genome alignments to six rhinolophid bats (boxes in the alignment net represent aligning sequence and connecting lines deletions or unaligning sequence). The grey box highlights a region that does not align between human and *Rhinolophus ferrumequinum*, because the *R. ferrumequinum* PacBio CLR-based assembly has a large 421,369 bp assembly gap in this locus. As a result, several ancestral mammal genes contained in this locus are missing from this assembly, which contributes to the slightly higher number of missing genes for *R. ferrumequinum* vs. other rhinolophid bats (Figure 1E). Consistent with PacBio HiFi-based assemblies tend to have higher contig N50 and N90 values (Figure 1C), the other four HiFi-based rhinolophid assemblies have a contiguous sequence in this locus without an assembly gap. *Rhinolophus sinicus*, which was assembled from Illumina short reads, has 24 smaller assembly gaps with sizes 15-1058 bp in this locus.

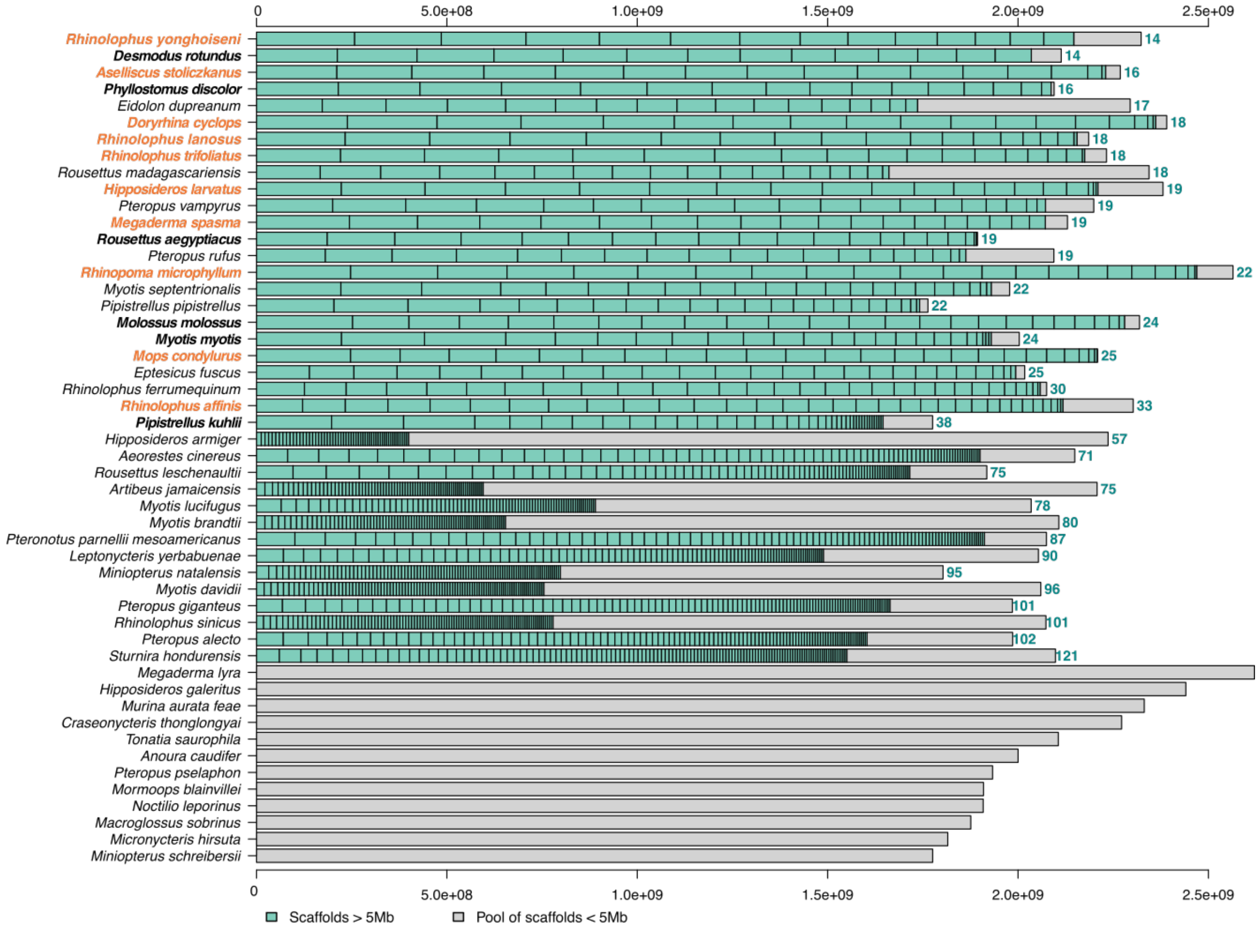

Supplementary Figure 3. Scaffold size distribution across 50 bat genomes. Visualization of scaffold lengths in 50 bat genomes. The ten newly-generated genomes in orange font, assemblies that are based on long reads are in bold. All assemblies are sorted by number of scaffolds larger than 50 Mb and by the median scaffold length. Scaffolds shorter than 50 Mb were pooled into the grey box on the right end.

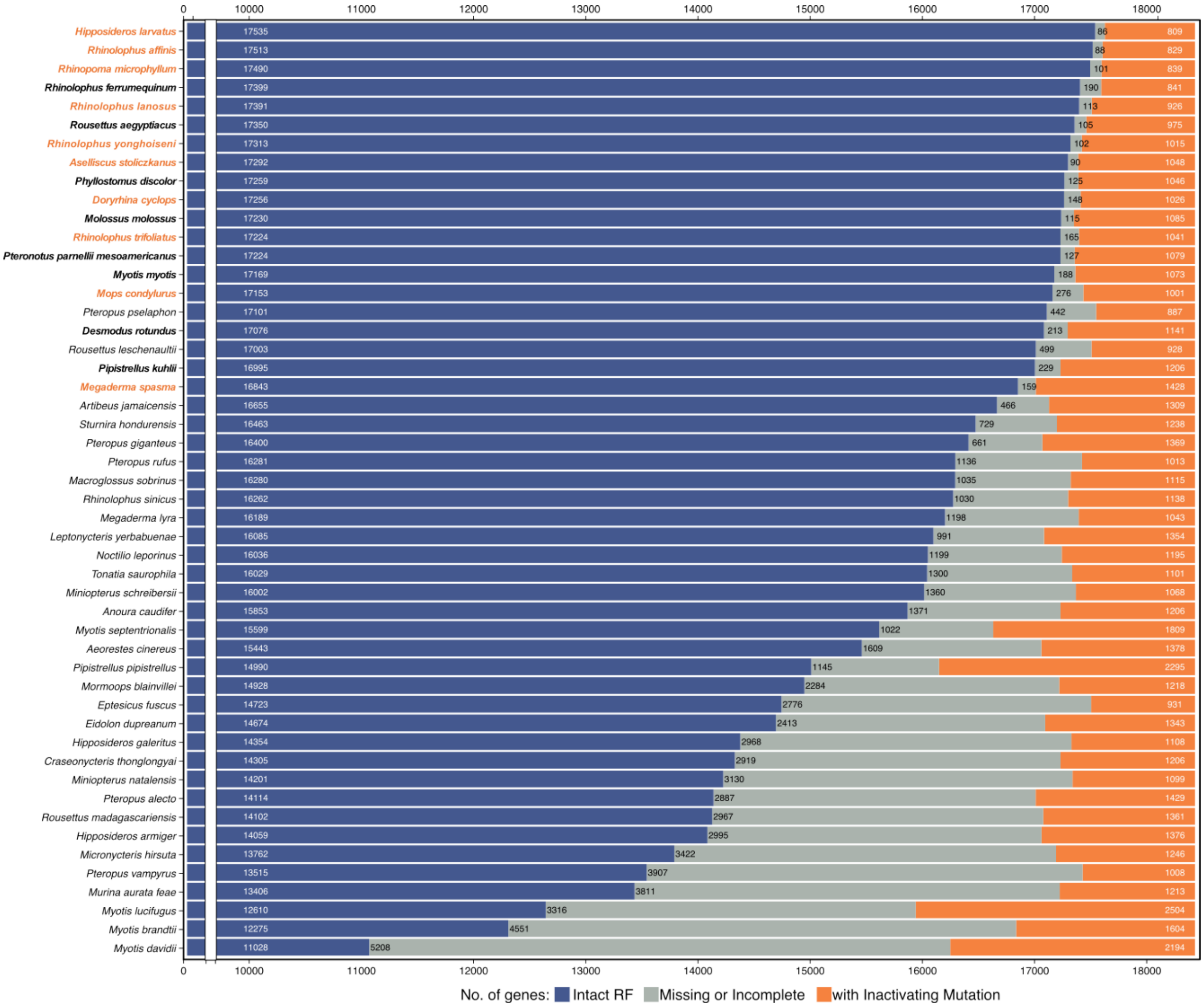

Supplementary Figure 4. Status of 18,430 ancestral mammalian genes in 50 bat genomes. This figure expands on Figure 1E by showing 50 bat genomes. Ancestral genes are classified by TOGA (using human hg38 as the reference) into those with an intact reading frame (blue), gene-inactivating mutations (orange) or missing or incomplete coding sequences due to assembly gaps or fragmentation (grey). The ten newly-generated genomes in orange font and assemblies that are based on long reads are in bold. All assemblies are sorted by the number of intact genes. Long-read based assemblies tend to have more intact genes and fewer genes with missing coding parts.

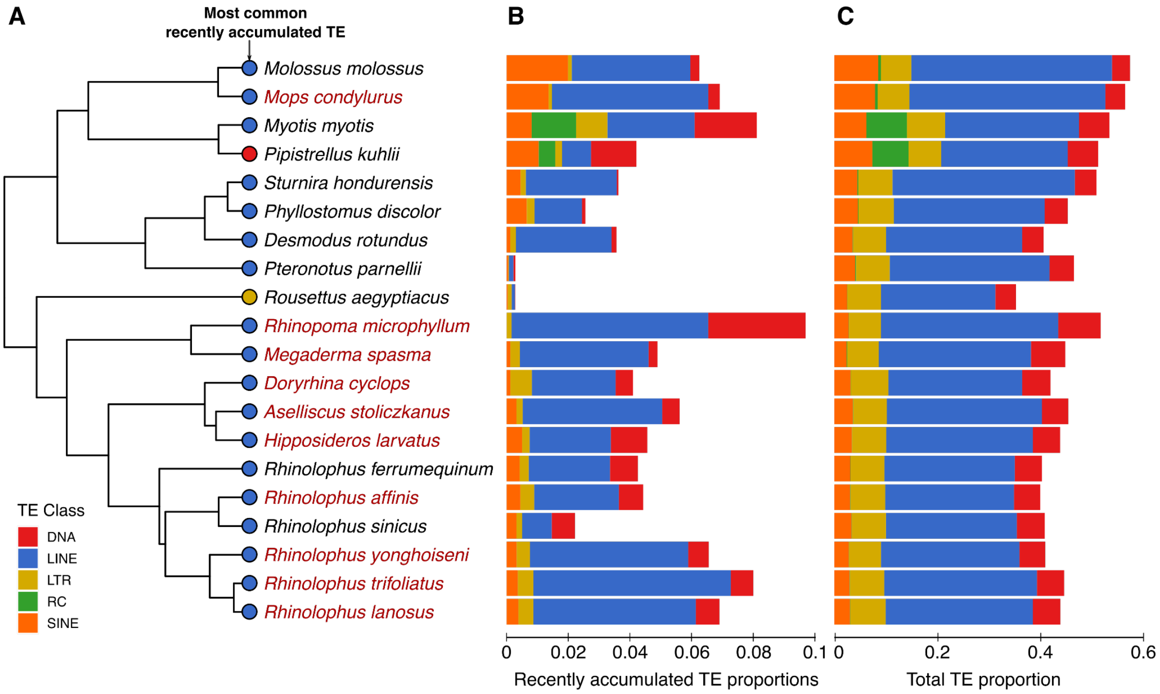

Supplementary Figure 5. Transposon content in the genomes of 20 bats.
(**A**) Phylogeny of examined species with circles at the tips indicating the class of the most common recently-accumulated TEs, defined as having <6% divergence from the respective consensus. The ten newly-generated genome assemblies are indicated in red font. (**B**) Bar plots indicating the class and proportion of recently-accumulated TEs. (**C**) Bar plots indicating the class and proportion of all TEs detected in the genomes.

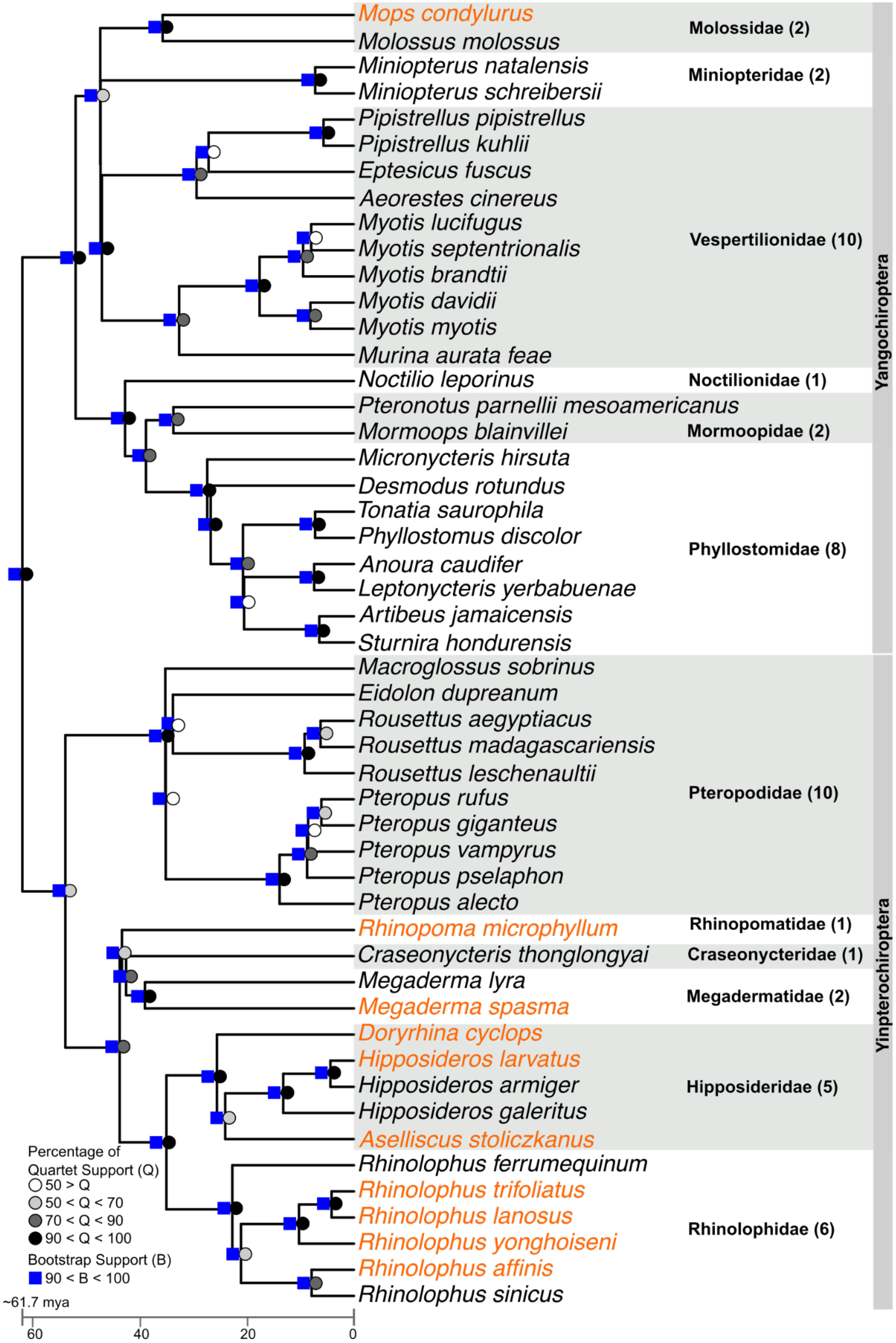

Supplementary Figure 6. Time-calibrated phylogeny of 50 bat species covering 12 families. Phylogenetic reconstruction was performed using 16,860 gene trees (representing 30,354,372 bp) estimated with RAxML followed by inferring a species tree using ASTRAL. Orthologous genes were inferred and annotated with TOGA using human as the reference. Multiple codon alignments were generated with TOGA's "exon-by-exon" alignment procedure with MACSE2. Node support values were estimated using quartet scores (circles) and 100 Transfer Bootstrap Expectation replicates (squares). The ten newly-generated genomes in orange font.

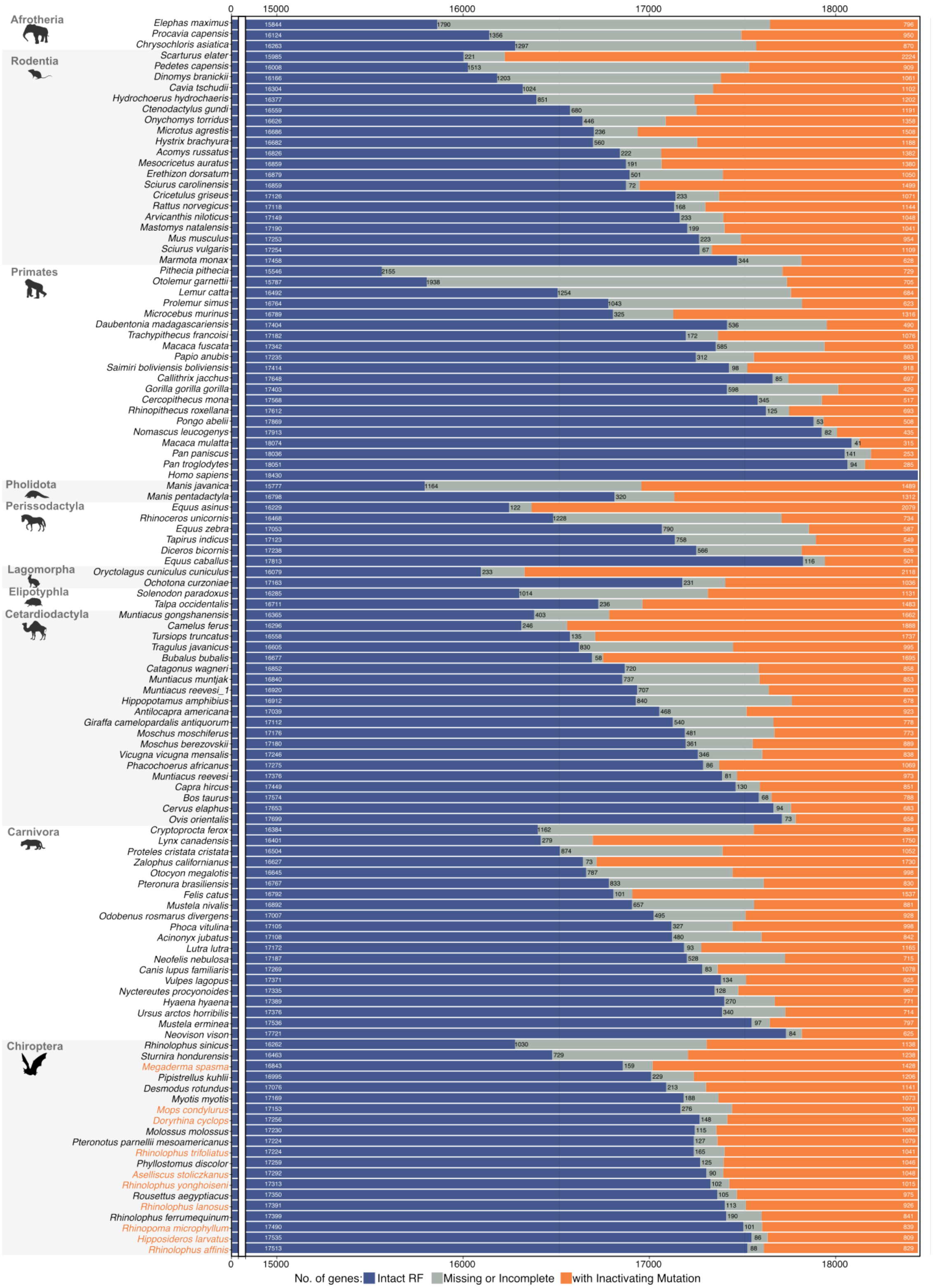

Supplementary Figure 7. Status of 18,430 ancestral mammalian genes in 115 mammalian genomes.

As in Figure 1E, ancestral genes are classified by TOGA into those with an intact reading frame (blue), gene-inactivating mutations (orange) or missing or incomplete coding sequences due to assembly gaps or fragmentation (grey). Here, all 115 mammals included in our selection screen are shown. In each mammalian group, genomes are reverse-sorted by the number of genes with intact reading frames. The ten newly-generated bat genomes in orange font.

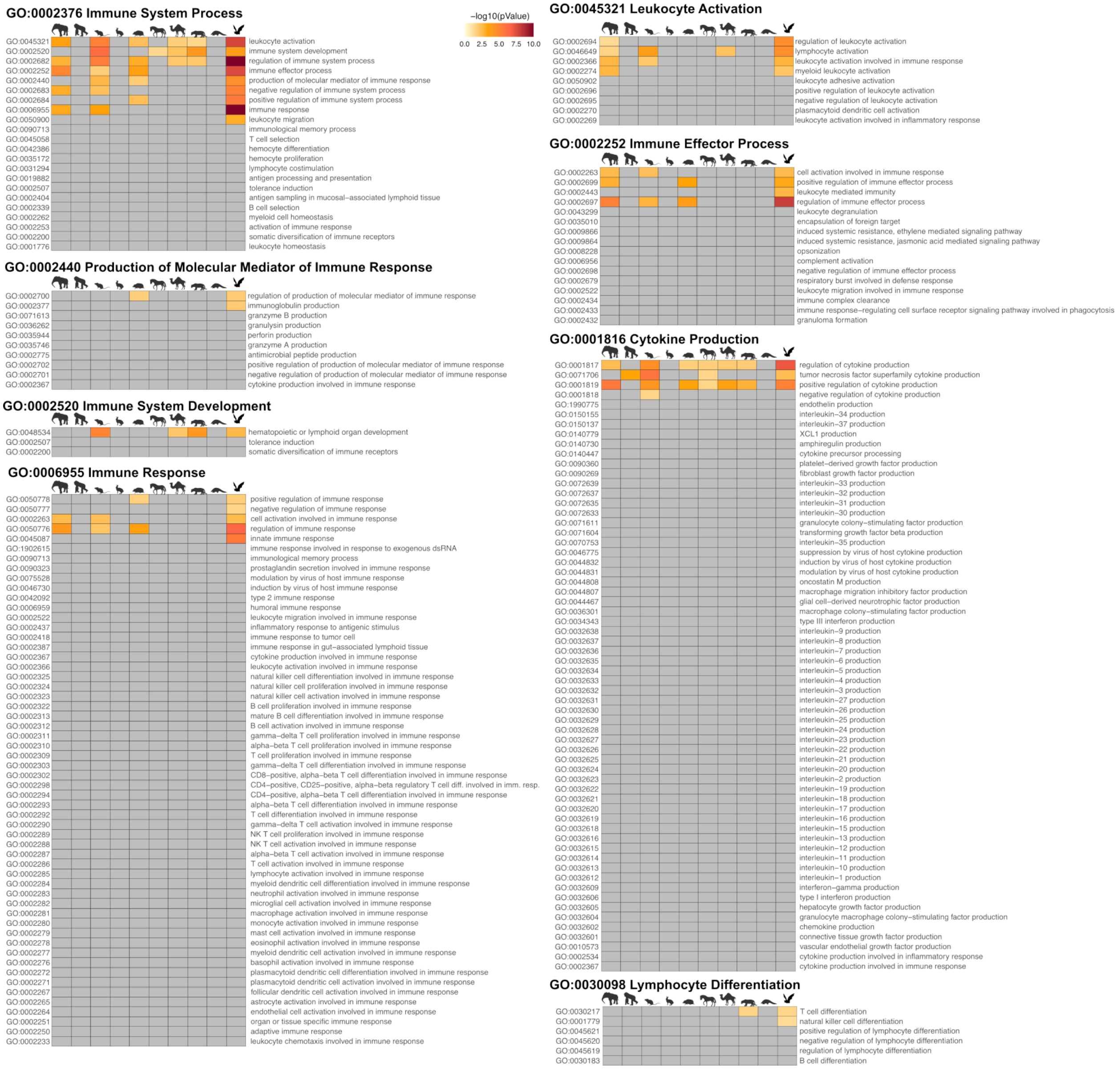

Supplementary Figure 8. Extended enrichment results for genes under selection and biological process GO terms.

Heatmaps showing enrichment results for genes under selection in each mammalian group, defined as genes for which at least one branch in the group showed a significant p-value for positive selection. Enrichments were performed in gProfiler. All child terms of high-level GO terms in Figure 2 are shown, also if they are not significant for any group. Columns represent mammalian groups (Afrotheria, Primates, Rodentia, Lagomorpha, Eulipotyphla, Perissodactyla, Cetartiodactyla, Carnivora, Pholidota, and Chiroptera). Rows represent children GO terms nested one level below the GO shown at the top of each plot. Colors indicate statistical significance based on -log$_{10}$(p-value) with light yellow indicating a low significance, dark red a strong significance and grey non-significance. Supplementary Table 7 provides the full gProfiler output, including all significant p-values for all groups.

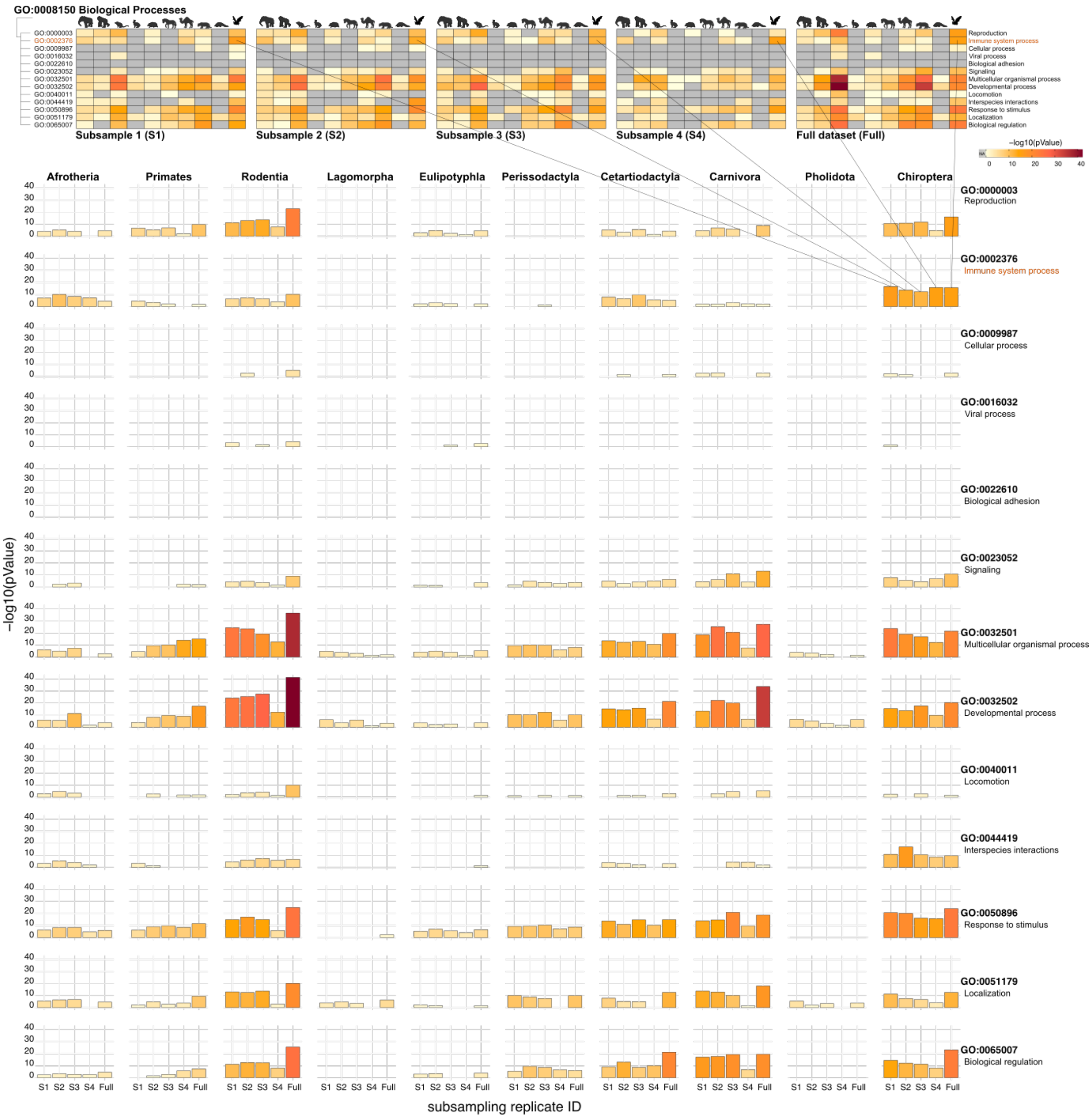

Supplementary Figure 9. Enrichments of genes under positive selection in four subsampled datasets for high-level GO terms of "Biological Process".

To explore whether functional enrichments of positively selected genes in mammalian clades are driven by individual species rather than being representative for the clade, we ran four additional screens for positive selection by subsampling 65 species from all 115 mammals, as explained in the Methods. In subsample 1-3, we randomly selected 10 of the 20 species in each clade that is represented by 20 species in the full dataset (Chiroptera, Primates, Rodentia, Cetartiodactyla, Carnivora). Subsample 4 includes all species left out in subsample 1 from the 20-species clades. Clades with less than 20 species were not subsampled. Enrichments were performed in gProfiler and categorized following the nested GO structure.

(A) Heatmaps show those direct child terms of GO Biological Process (GO:0008150) that have a significant p-value in at least one clade. Columns represent mammalian groups (Afrotheria, Primates, Rodentia, Lagomorpha, Eulipotyphla, Perissodactyla, Cetartiodactyla, Carnivora, Pholidota, and Chiroptera). Rows represent child terms of GO:0008150. Colors indicate statistical significance based on $-\log_{10}$(p-value) with light yellow indicating a low significance, dark red strong significance and grey non-significance.

(B) For a direct comparison of the enrichment significance, bar plots visualize the $-\log_{10}$(p-value) for the four subsamples (first four bars) in comparison to the full dataset (fifth bar). For consistency, the bar color is the same as in (A).

Importantly, the chiropteran enrichments “immune system process” and “response to stimulus” are robustly observed across the subsamples. For “immune system process”, no other mammalian group exhibits an enrichment as strong as in Chiroptera.

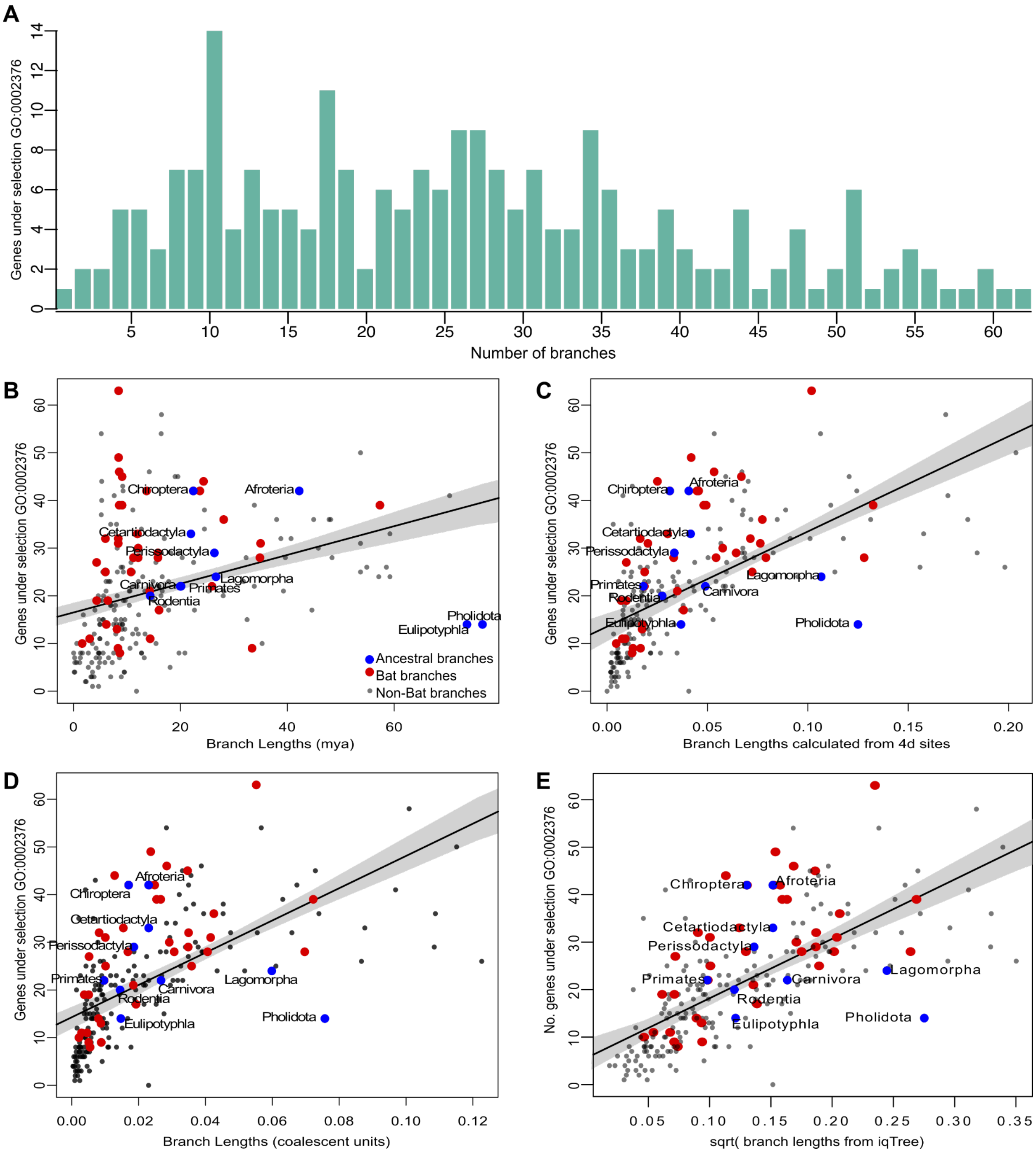

Supplementary Figure 10. Correlation between branch length and number of genes under selection in "Immune System Process" (GO:0002376).

(A) Distribution of the number of genes that are under selection in a given number of branches, considering all 228 branches in the 115-species tree.

(B-I) Dispersion plots of correlation between different measures of branch lengths and the number of genes under selection. For branch lengths, we used three independent estimations:

(B) millions of years taken from our time-calibrated phylogeny inferred using treePL and fossil calibrations (Supplementary Table 4),

(C) number of substitutions per neutral site estimated from 4D sites using phyloFit,
(D) number of substitutions per site estimated from coding regions using IQTREE,
(E) transformed branch lengths as the square-root of the number of substitutions per site estimated from coding regions using IQTREE.
Akaike's information criterion (AIC) indicates that the model in (E) fits the data best (Supplementary Table 9).

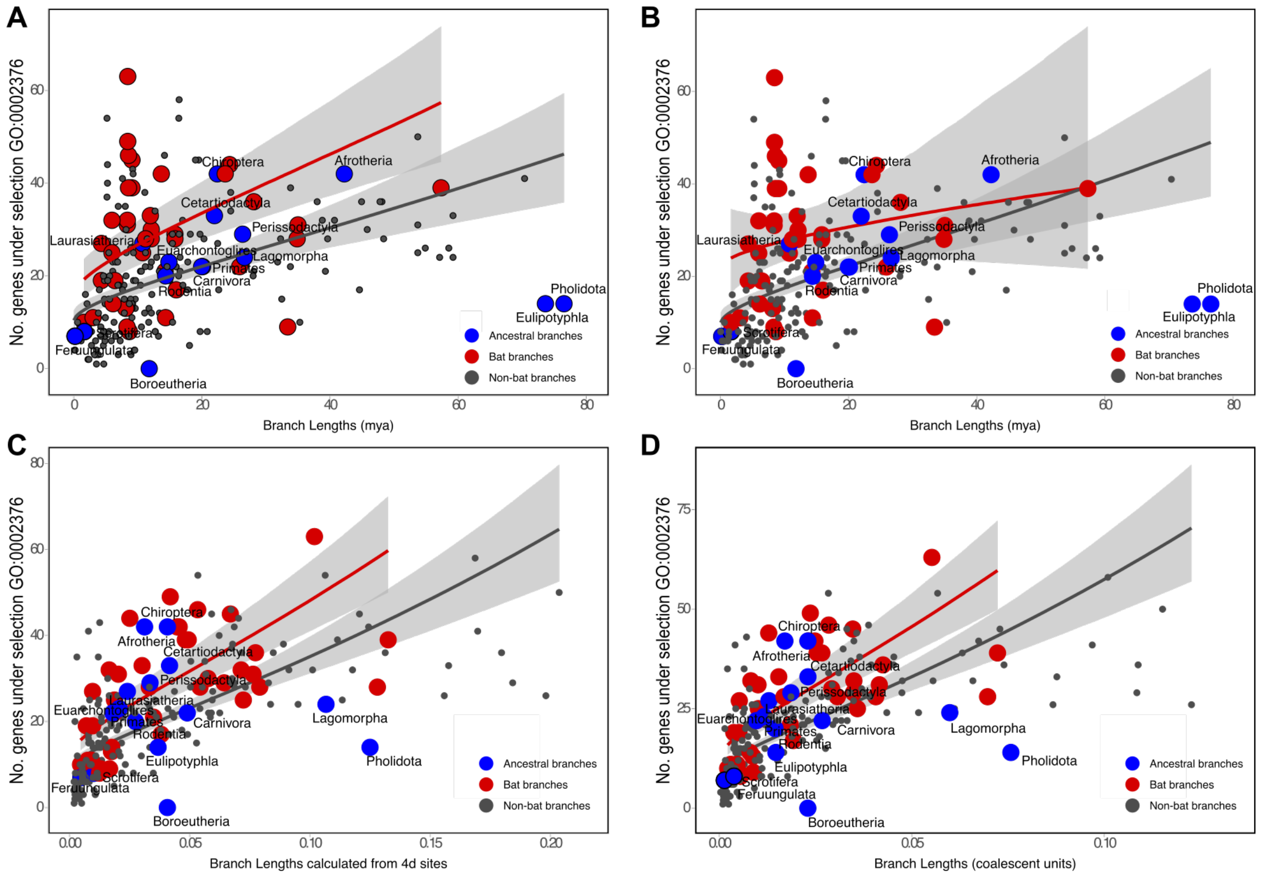

Supplementary Figure 11. Model selection with two intercepts.

To determine whether the number of immune genes under selection is higher in bats than in other mammals, we introduced a categorical variable, corresponding to taxonomy (bats and non-bats) and fit a series of negative binomial regressions where two intercepts and two slopes would be allowed in the models.

(A) negative binomial, two-intercept model of square-root transformed millions of years from a time-calibrated phylogeny inferred using treePL and fossil calibrations (Supplementary Table 4)

(B) negative binomial, two-intercept and two slope model of square-root transformed millions of years from a time-calibrated phylogeny inferred using treePL and fossil calibrations (Supplementary Table 4)

(C) negative binomial, two-intercept model of square-root transformed number of substitutions per neutral site estimated from 4D sites using phyloFit

(D) negative binomial, two-intercept model of square-root transformed number of substitution per site estimated from coding regions using IQTREE.

The best-fit model has two intercepts corresponding to bats and non-bats, but a single slope. These results robustly show that bats had a higher number of immune-related genes under selection, since early evolutionary times.

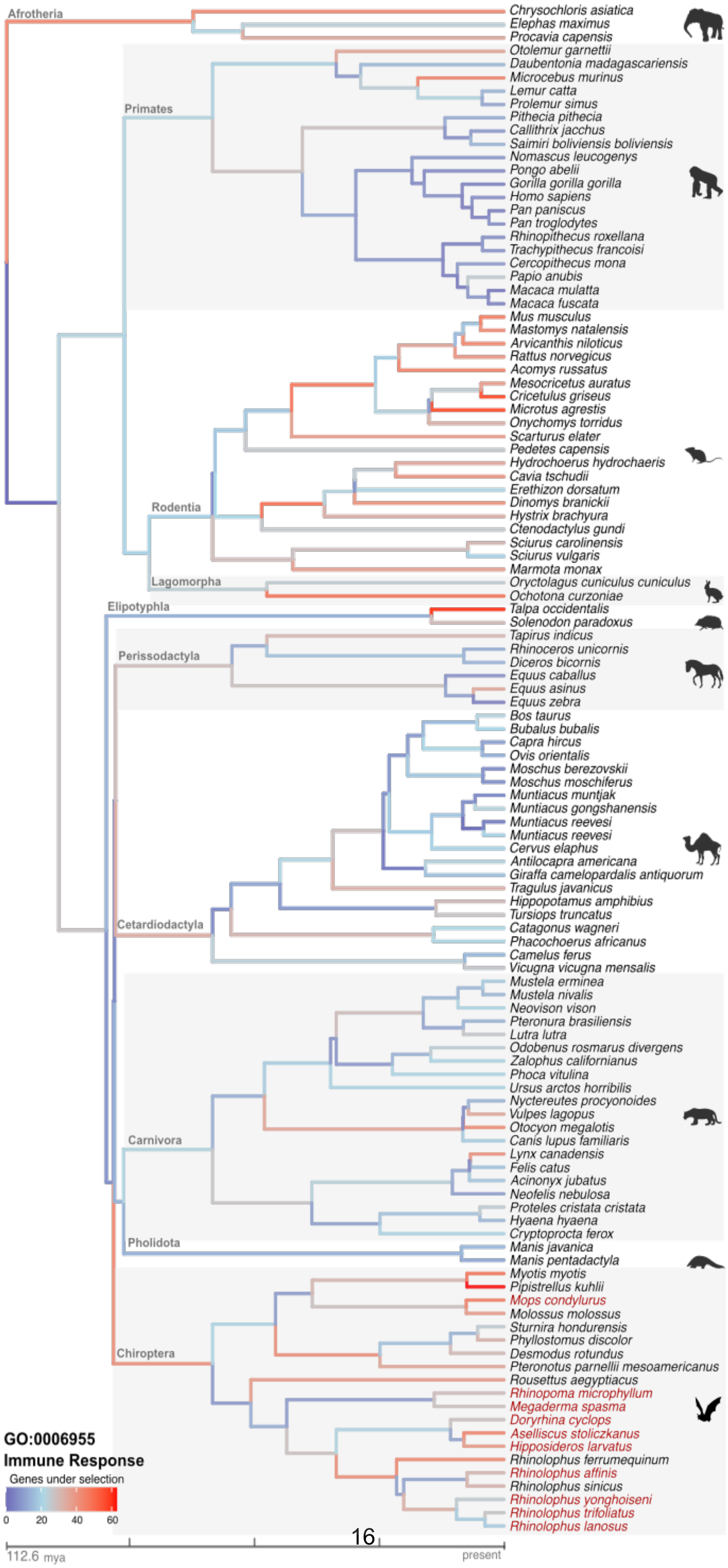
Afrotheria
Chrysochloris asiatica
Elephas maximus
Procavia capensis
Primates
Otolemur garnettii
Daubentonia madagascariensis
Microcebus murinus
Lemur catta
Prolemur simus
Pithecia pithecia
Callithrix jacchus
Saimiri boliviensis boliviensis
Nomascus leucogenys
Pongo abelii
Gorilla gorilla gorilla
Homo sapiens
Pan paniscus
Pan troglodytes
Rhinopithecus roxellana
Trachypithecus francoisi
Cercopithecus mona
Papio anubis
Macaca mulatta
Macaca fuscata
Rodentia
Mus musculus
Mastomys natalensis
Arvicanthis niloticus
Rattus norvegicus
Acomys russatus
Mesocricetus auratus
Cricetulus griseus
Microtus agrestis
Onychomys torridus
Scarturus elater
Pedetes capensis
Hydrochoerus hydrochaeris
Cavia tschudii
Erethizon dorsatum
Dinomys branickii
Hystrix brachyura
Ctenodactylus gundi
Sciurus carolinensis
Sciurus vulgaris
Marmota monax
Lagomorpha
Oryctolagus cuniculus cuniculus
Ochotona curzoniae
Elipotyphla
Talpa occidentalis
Solenodon paradoxus
Perissodactyla
Tapirus indicus
Rhinoceros unicornis
Diceros bicornis
Equus caballus
Equus asinus
Equus zebra
Cetardiodactyla
Bos taurus
Bubalus bubalis
Capra hircus
Ovis orientalis
Moschus berezovskii
Moschus moschiferus
Muntiacus muntjak
Muntiacus gongshanensis
Muntiacus reevesi
Muntiacus reevesi
Cervus elaphus
Antilocapra americana
Giraffa camelopardalis antiquorum
Tragulus javanicus
Hippopotamus amphibius
Tursiops truncatus
Catagonus wagneri
Phacochoerus africanus
Camelus ferus
Vicugna vicugna mensalis
Carnivora
Mustela erminea
Mustela nivalis
Neovison vison
Pteronura brasiliensis
Lutra lutra
Odobenus rosmarus divergens
Zalophus californianus
Phoca vitulina
Ursus arctos horribilis
Nyctereutes procyonoides
Vulpes lagopus
Otocyon megalotis
Canis lupus familiaris
Lynx canadensis
Felis catus
Acinonyx jubatus
Neofelis nebulosa
Proteles cristata cristata
Hyaena hyaena
Cryptoprocta ferox
Pholidota
Manis javanica
Manis pentadactyla
Chiroptera
Myotis myotis
Pipistrellus kuhlii
Mops condylurus
Molossus molossus
Sturnira hondurensis
Phyllostomus discolor
Desmodus rotundus
Pteronotus parnellii mesoamericanus
Rousettus aegyptiacus
Rhinopoma microphyllum
Megaderma spasma
Doryrhina cyclops
Aselliscus stoliczkanus
Hipposideros larvatus
Rhinolophus ferrumequinum
Rhinolophus affinis
Rhinolophus sinicus
Rhinolophus yonghoiseni
Rhinolophus trifoliatus
Rhinolophus lanosus
GO:0006955
Immune Response
Genes under selection
0
20
40
60
112.6 mya
present

Supplementary Figure 12. Per-branch signal of "Immune Response" (GO:0006955) selection on the phylogeny for 115 mammals.

Time-calibrated phylogeny with branches color-coded by the absolute number of genes under selection annotated with the GO term "Immune Response" (GO:0006955). The time scale at the bottom represents divergence times in millions of years ago, and the color scale goes from 0 genes under selection (blue) to the maximum number of genes under selection in a single branch (red). Ancestral branches for mammalian groups are labeled as Afrotheria, Primates, Rodentia, Lagomorpha, Eulipotyphla, Perissodactyla, Cetartiodactyla, Carnivora, Pholidota, and Chiroptera.

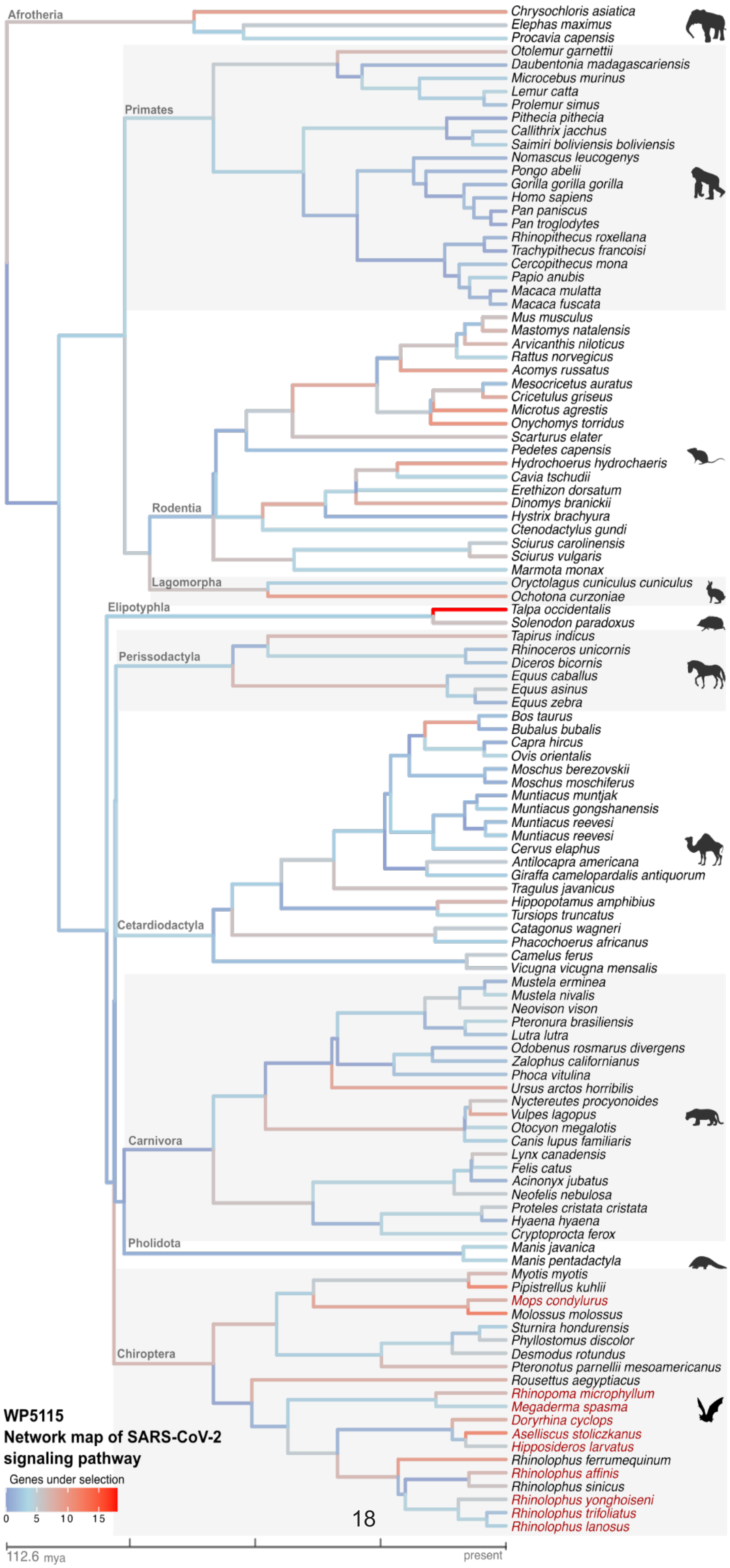

WP5115
Network map of SARS-CoV-2 signaling pathway

Supplementary Figure 13. Per-branch signal of “Network map of SARS-CoV-2 signaling pathway” (WP5115) selection on the phylogeny for 115 mammals.
Time-calibrated phylogeny with branches color-coded by the absolute number of genes under selection that are part of the Network map of the “SARS-CoV-2 signaling pathway” (Homo sapiens; https://www.wikipathways.org/index.php/Pathway:WP5115, last access, July 20th, 2022). The time scale at the bottom represents divergence times in millions of years ago, and the color scale goes from 0 genes under selection (blue) to the maximum number of genes under selection in a single branch (red). Ancestral branches for mammalian groups are labeled as Afrotheria, Primates, Rodentia, Lagomorpha, Eulipotyphla, Perissodactyla, Cetartiodactyla, Carnivora, Pholidota, and Chiroptera.

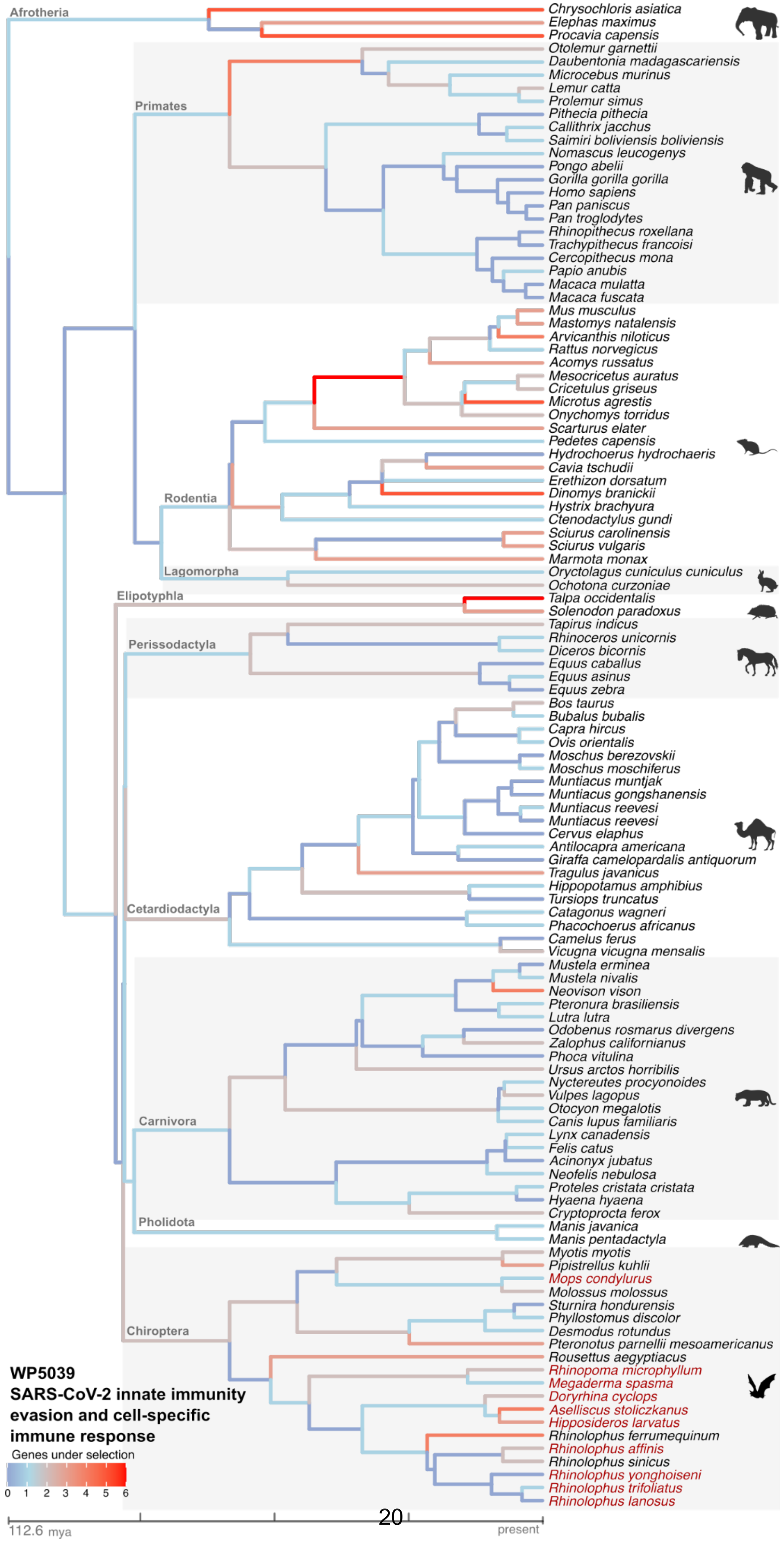
Afrotheria
Chrysochloris asiatica
Elephas maximus
Procavia capensis
Primates
Otolemur garnettii
Daubentonia madagascariensis
Microcebus murinus
Lemur catta
Prolemur simus
Pithecia pithecia
Callithrix jacchus
Saimiri boliviensis boliviensis
Nomascus leucogenys
Pongo abelii
Gorilla gorilla gorilla
Homo sapiens
Pan paniscus
Pan troglodytes
Rhinopithecus roxellana
Trachypithecus francoisi
Cercopithecus mona
Papio anubis
Macaca mulatta
Macaca fuscata
Rodentia
Mus musculus
Mastomys natalensis
Arvicanthis niloticus
Rattus norvegicus
Acomys russatus
Mesocricetus auratus
Cricetulus griseus
Microtus agrestis
Onychomys torridus
Scarturus elater
Pedetes capensis
Hydrochoerus hydrochaeris
Cavia tschudii
Erethizon dorsatum
Dinomys branickii
Hystrix brachyura
Ctenodactylus gundi
Sciurus carolinensis
Sciurus vulgaris
Marmota monax
Lagomorpha
Oryctolagus cuniculus cuniculus
Ochotona curzoniae
Elipotyphla
Talpa occidentalis
Solenodon paradoxus
Perissodactyla
Tapirus indicus
Rhinoceros unicornis
Diceros bicornis
Equus caballus
Equus asinus
Equus zebra
Cetardiodactyla
Bos taurus
Bubalus bubalis
Capra hircus
Ovis orientalis
Moschus berezovskii
Moschus moschiferus
Muntiacus muntjak
Muntiacus gongshanensis
Muntiacus reevesi
Muntiacus reevesi
Cervus elaphus
Antilocapra americana
Giraffa camelopardalis antiquorum
Tragulus javanicus
Hippopotamus amphibius
Tursiops truncatus
Catagonus wagneri
Phacochoerus africanus
Camelus ferus
Vicugna vicugna mensalis
Carnivora
Mustela erminea
Mustela nivalis
Neovison vison
Pteronura brasiliensis
Lutra lutra
Odobenus rosmarus divergens
Zalophus californianus
Phoca vitulina
Ursus arctos horribilis
Nyctereutes procyonoides
Vulpes lagopus
Otocyon megalotis
Canis lupus familiaris
Lynx canadensis
Felis catus
Acinonyx jubatus
Neofelis nebulosa
Proteles cristata cristata
Hyaena hyaena
Cryptoprocta ferox
Pholidota
Manis javanica
Manis pentadactyla
Chiroptera
Myotis myotis
Pipistrellus kuhlii
Mops condylurus
Molossus molossus
Sturnira hondurensis
Phyllostomus discolor
Desmodus rotundus
Pteronotus parnellii mesoamericanus
Rousettus aegyptiacus
Rhinopoma microphyllum
Megaderma spasma
Dorythina cyclops
Aselliscus stoliczkanus
Hipposideros larvatus
Rhinolophus ferrumequinum
Rhinolophus affinis
Rhinolophus sinicus
Rhinolophus yonghoiseni
Rhinolophus trifoliatus
Rhinolophus lanosus
WP5039
SARS-CoV-2 innate immunity evasion and cell-specific immune response
Genes under selection
0 1 2 3 4 5 6
112.6 mya
present

Supplementary Figure 14. Per-branch signal of “SARS-CoV-2 innate immunity evasion and cell-specific immune response” (WP5039) selection on phylogeny for 115 mammals. Time-calibrated phylogeny with branches color-coded by the absolute number of genes under selection that are part of the “SARS-CoV-2 innate immunity evasion and cell-specific immune response” (Homo sapiens; https://www.wikipathways.org/index.php/Pathway:WP5039, last access, July 20th, 2022). The time scale at the bottom represents divergence times in millions of years ago, and the color scale goes from 0 genes under selection (blue) to the maximum number of genes under selection in a single branch (red). Ancestral branches for mammalian groups are labeled as Afrotheria, Primates, Rodentia, Lagomorpha, Eulipotyphla, Perissodactyla, Cetartiodactyla, Carnivora, Pholidota, and Chiroptera.

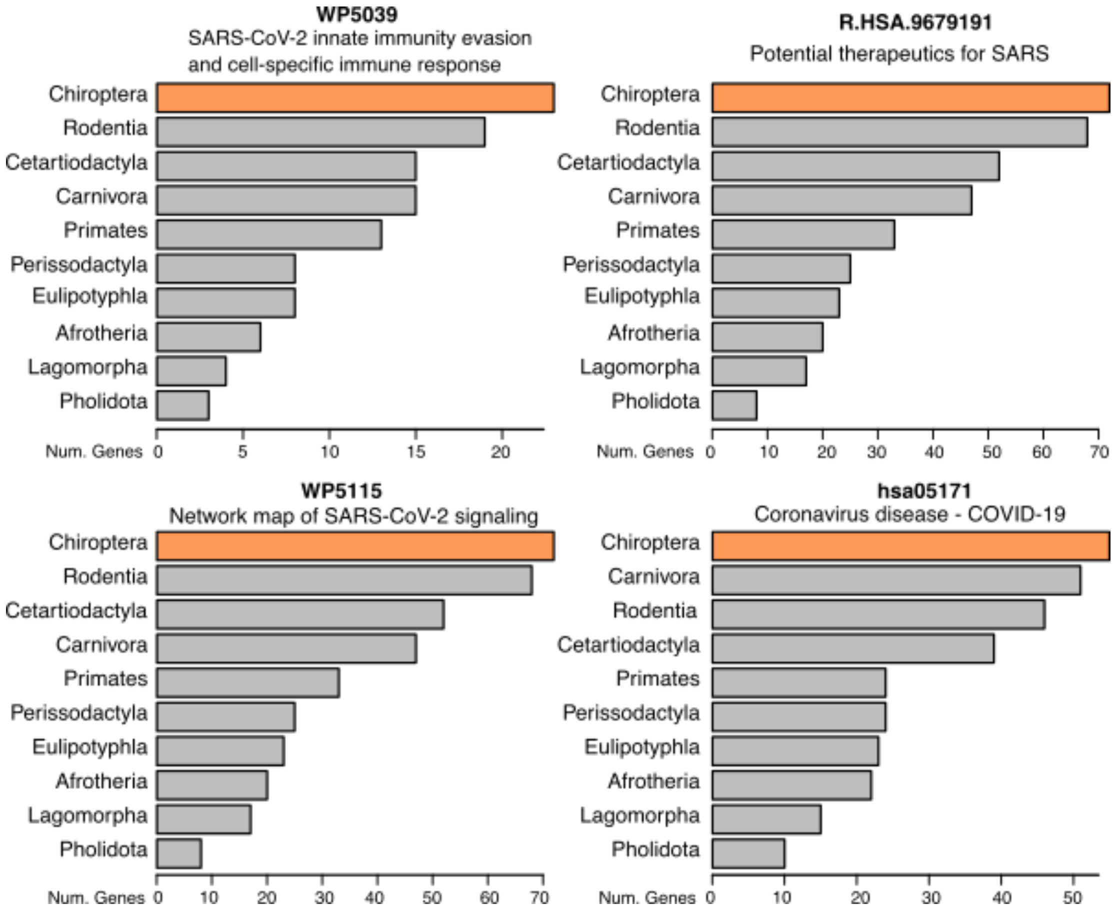

Supplementary Figure 15. Genes under positive selection in SARS-CoV-2 related pathways.

Absolute number of genes under positive selection in different mammalian orders (at least one branch has a significant p-value) that are involved in pathways with relevance for SARS-CoV-2 and COVID-19. Pathway data was taken from WikiPathways (https://www.wikipathways.org/index.php/Pathway:WP5039, https://www.wikipathways.org/index.php/Pathway:WP5115), Reactome (https://www.wikipathways.org/index.php/Pathway:WP5039), and KEGG pathways (https://www.genome.jp/pathway/hsa05171), in all cases last access on July 20th, 2022. Chiroptera consistently have the highest number of selected genes in these gene sets.

Supplementary Figure 16. Enrichments of genes under positive selection in four subsampled datasets for child terms of “Immune System Process”.

Selection and enrichment analyses for the four subsampled datasets (65 genomes each) in comparison with the full dataset (115 genomes) for the child terms of “Immune System Process” (GO:0002376). Visualization and legend as in Supplementary Figure 9. Genes positively selected in Chiroptera robustly show a strong enrichment in “Immune Response” and “Regulation of Immune System Process”, where the enrichments are higher than in any other mammalian group.

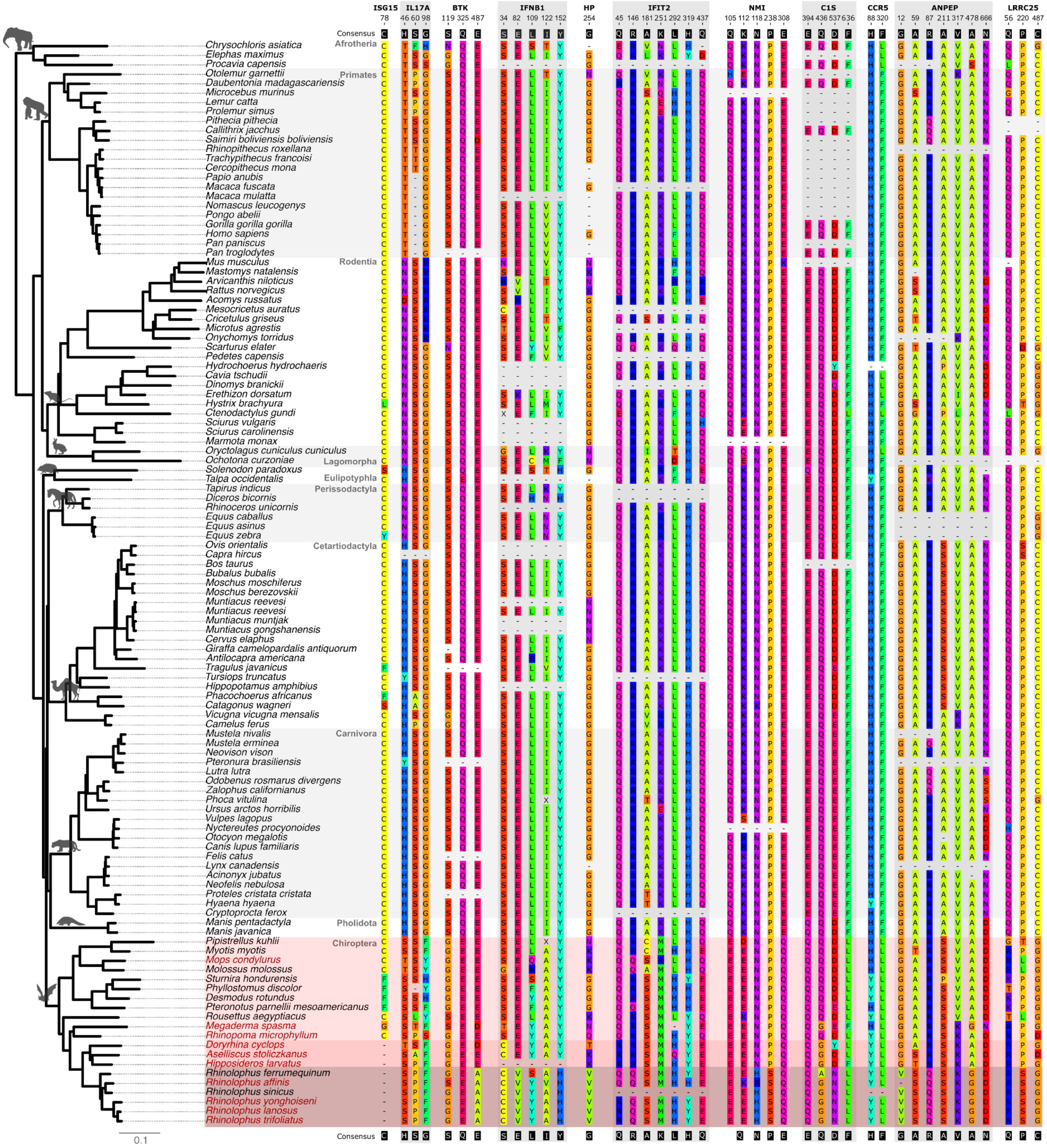

Supplementary Figure 17. (continued below)

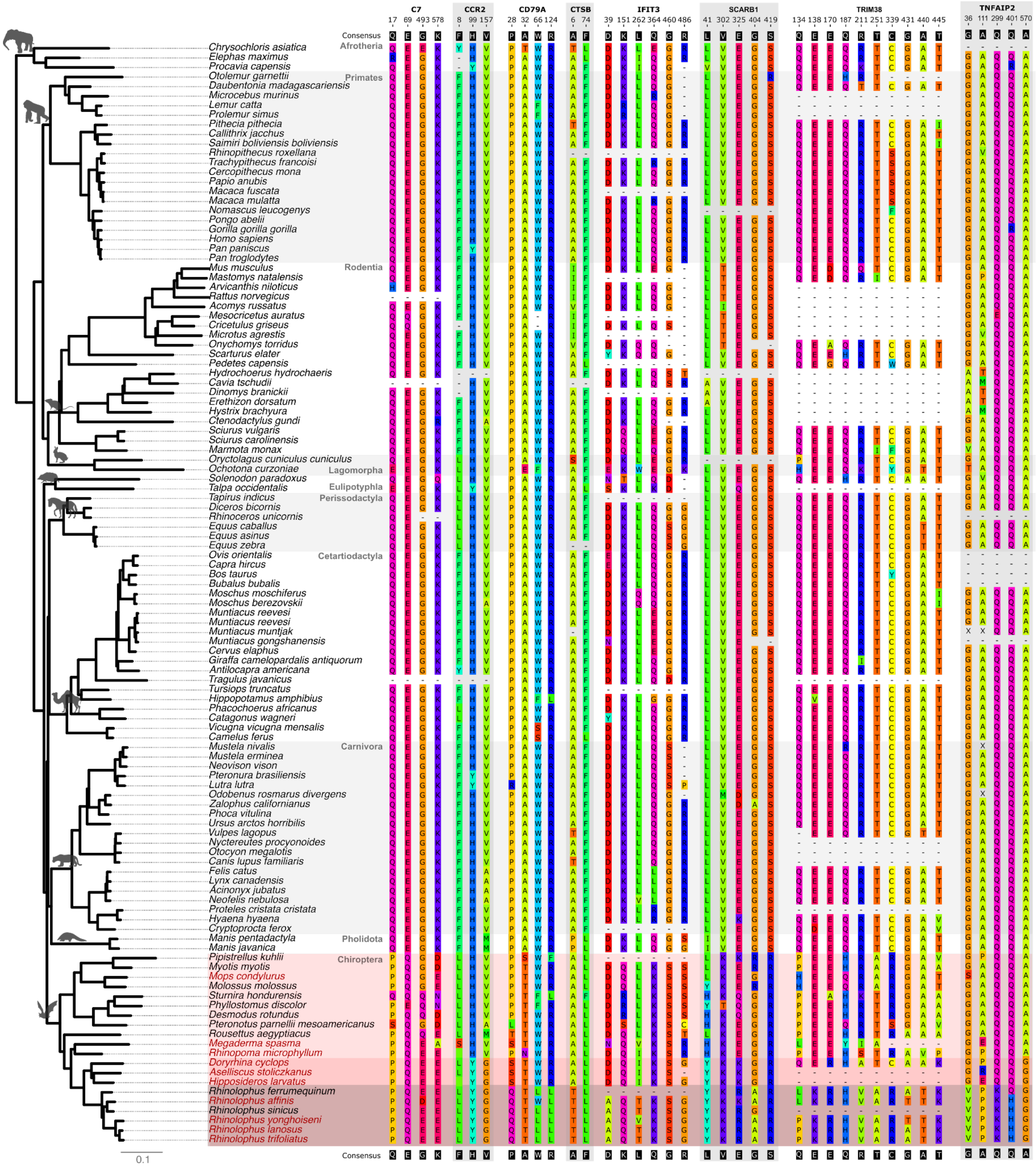

Supplementary Figure 17. Amino acid alignments highlighting residue changes in bats. Protein alignments of ISG15 and of genes under selection, highlighting residues with bat-specific mutations. Residue numbers correspond to positions in the filtered alignments we used as input for aBSREL. Since we only included 1:1 orthologous genes with intact reading frames (TOGA status intact, meaning the middle 80% of the reading frame lacks inactivating mutations) in the screen, dashes can correspond to duplicated genes, inactivating mutations near the N- or C-terminus, or missing genomic sequence. Full raw and filtered alignments are available at http://genome.senckenberg.de/download/Bat1KImmune/.

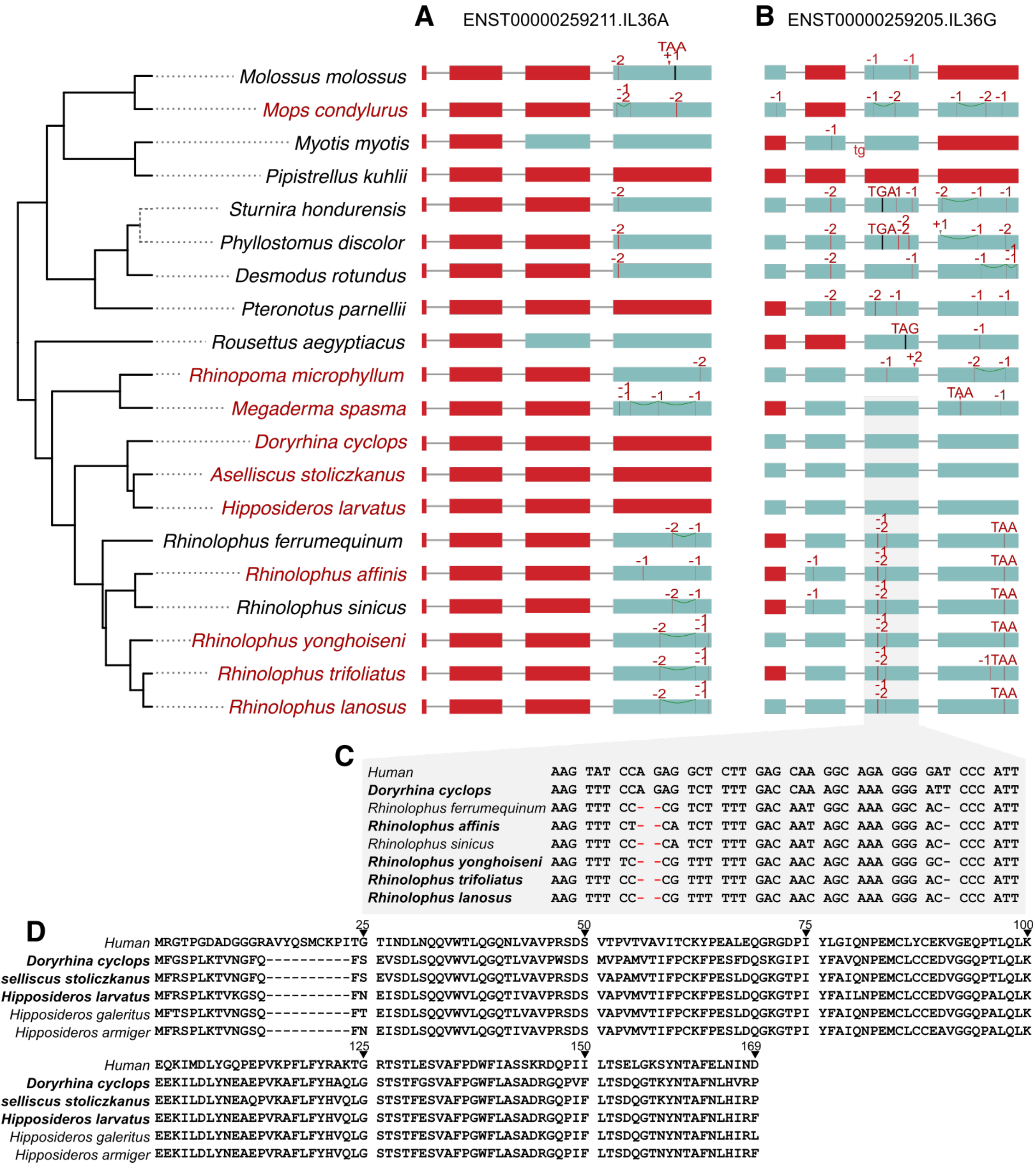

Supplementary Figure 18. Inactivating mutations and deletions of *IL36A* and *IL36G* in bats. (**A**) The deletion of *IL36A* exons 1-3 shares the same downstream breakpoint in rhinolophid bats and in *Rhinopoma muscatellum*, which indicates that this deletion already occurred in the common ancestor of *Hipposideridae*, *Megadermatidae*, *Rhinolophidae*, and *Rhinopomatidae* (*Rhinolophoidea* superfamily). Thus, loss of *IL36A* predates the split of *Rhinolophoidea.* In *Megaderma spasma* and *R. yonghoiseni*, additional deletions occurred secondarily. All analyzed hipposiderid bats additionally exhibit a genomic rearrangement in this locus and do not exhibit any traces of *IL36A*.

(**B**) Extending previous findings (Jebb et al. 2020), *IL36G* was independently lost in several bat families. Shared frameshifts in exon 3 indicate that *IL36G* was inactivated in the common ancestor of rhinolophid bats. In contrast, *IL36G* maintains an intact reading frame in *Hipposideridae*.

(**C**) Codon alignment of *IL36G* exon 3 showing the shared -2 and -1 bp frameshifting deletions (red font) in rhinolophid bats in comparison with human and hipposiderid bats (represented by *Doryrhina cyclops*).

(**D**) Amino acid alignment of IL36G of human and hipposiderid bats shows divergence at the N-terminus. However, the IL36G protein shows many conserved residues, indicating that the gene encodes a functional protein in hipposiderid bats.

In (A) and (B), coding exons are represented as boxes, superimposed with inactivating mutations. Vertical red lines are frameshifting deletions and arrowheads indicate frameshifting insertions. Red boxes indicate complete exon deletions. The size of deletions or insertions are given on top of the mutation. Premature stop codons are shown as black vertical lines with the corresponding triplet. An acceptor splice site mutation (tg) is shown by red letters at the beginning of *IL36G* exon 3.

Genome assemblies produced in this study are in red font in (A) and (B) and in bold font in (C) and (D).

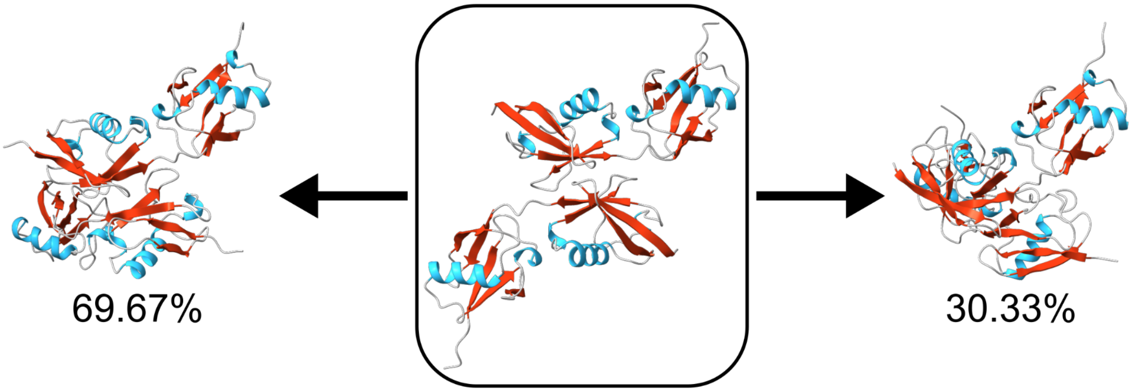

Supplementary Figure 19. Conformations of putative dimers of the ISG15 of *Rhinolophus sinicus*.

The dimer that we estimated with AlphaFold is circled, whereas the other dimers are representative conformations, observed during 3 µs of molecular dynamics simulations (see Methods). The lack of the disulfide bond appears to result in an unstable dimer that adopts two major conformations that differ considerably in the spatial arrangement of the monomers, both from each other and from the starting AlphaFold structure. Helices are shown in cyan, whereas β-strands in red. The percentages correspond to the proportion of each conformation across the simulations. The figure was rendered with UCSF ChimeraX v.1.2 (Pettersen et al. 2021).

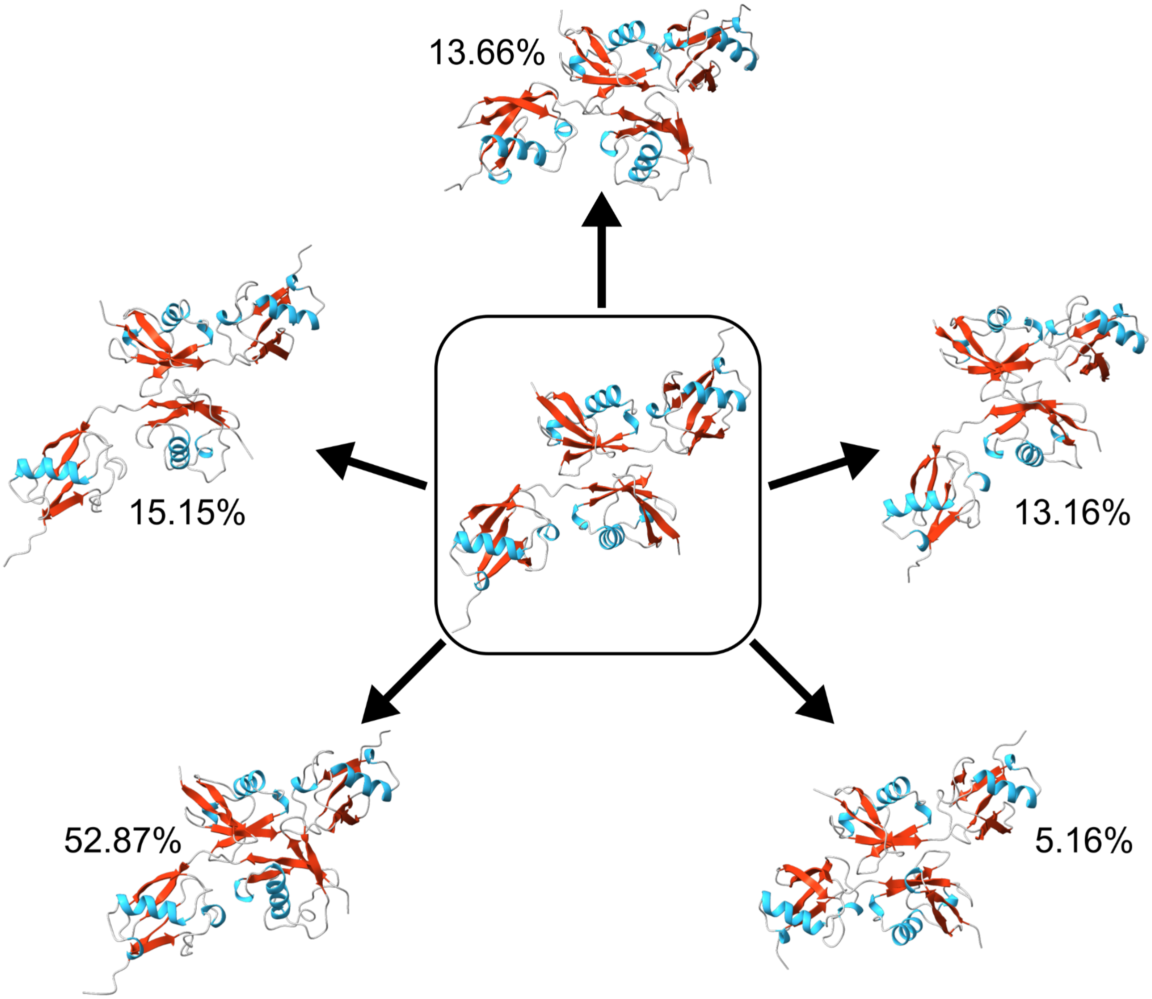

Supplementary Figure 20. Conformations of putative dimers of the ISG15 of *Doryrhina cyclops*.

The dimer that we estimated with AlphaFold is circled, whereas the other dimers are representative conformations, observed during 3 μs of molecular dynamics simulations (see Methods). The lack of the disulfide bond appears to result in an unstable dimer that adopts a range of conformations, with remarkable differences in the spatial arrangement of the monomers. Helices are shown in cyan, whereas β-strands in red. The percentages correspond to the proportion of each conformation across the simulations. The figure was rendered with UCSF ChimeraX v.1.2 (Pettersen et al. 2021).

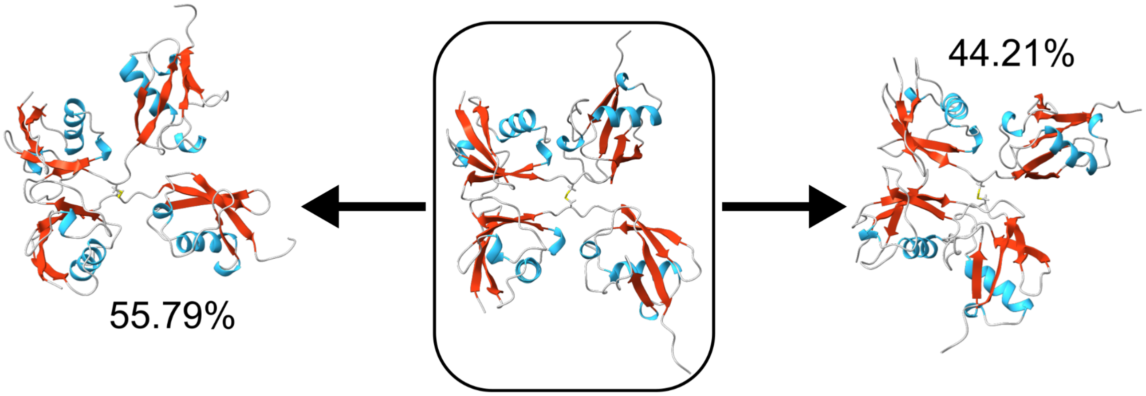

Supplementary Figure 21. Conformations of putative dimers of human ISG15.

The dimer that we estimated with AlphaFold is circled, whereas the two other dimers are representative conformations, observed during 3 μs of molecular dynamics simulations (see Methods). The dimer appears stable, with monomers being able to only slightly rotate around the disulfide bond. Helices are shown in cyan, whereas β-strands in red. The percentages correspond to the proportion of each conformation across the simulations. The figure was rendered with UCSF ChimeraX v.1.2 (Pettersen et al. 2021).

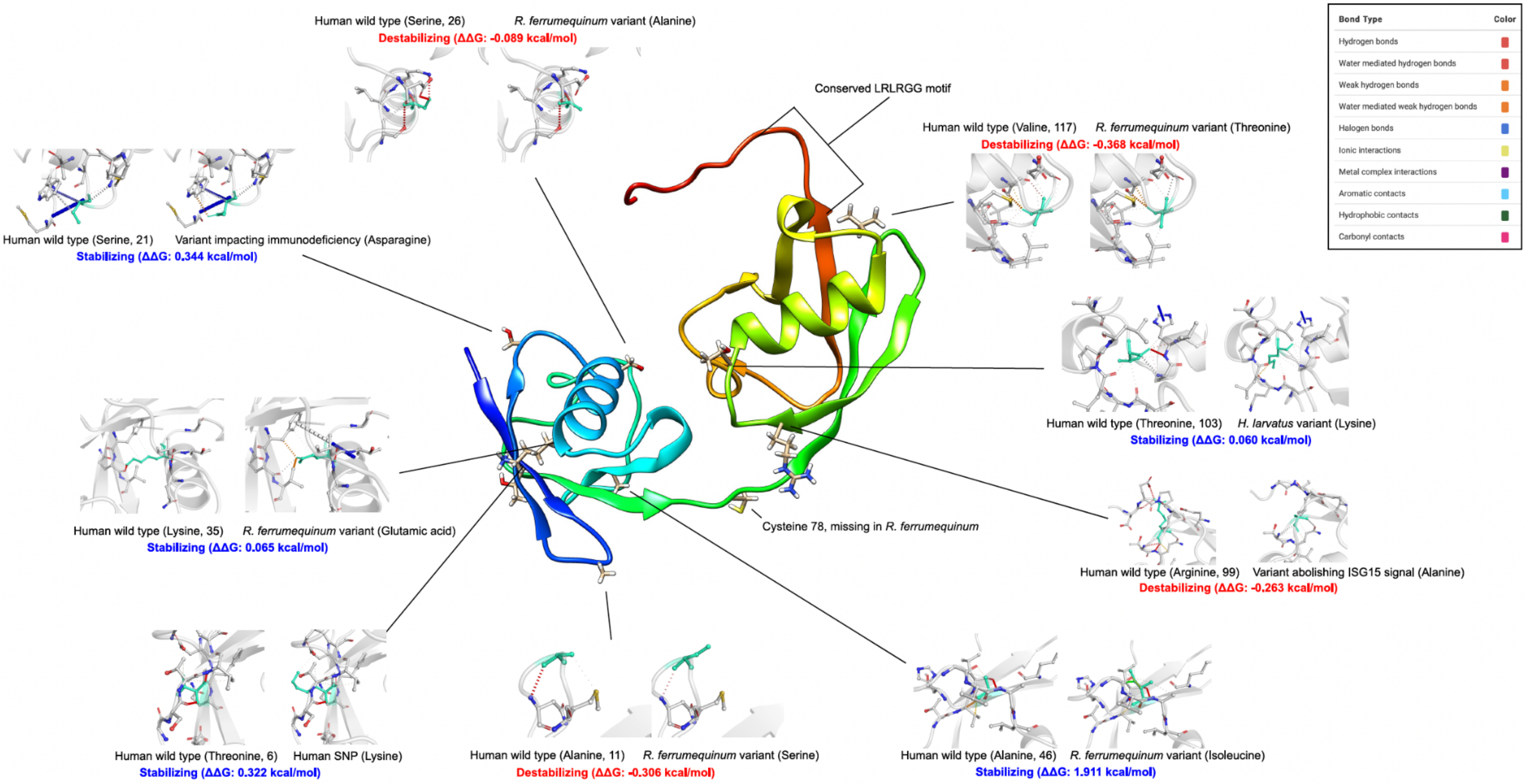

Supplementary Figure 22. ISG15 protein structure predicted with I-TASSER

Nine key sites showing bat-specific mutations are highlighted relative to the human wild-type (T6K, A11S, S21N, S26A, K35E, A46I, R99A, T103K,V117T/M).

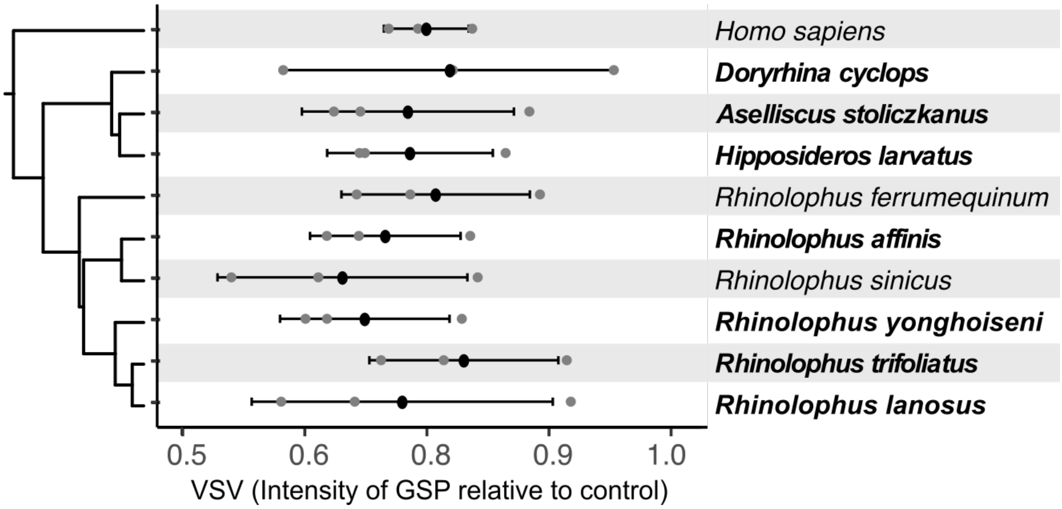

Supplementary Figure 23. Viral load in VSV-infected HEK293 cells with bat-ISG15 constructs.

Viral load for the data shown in Fig. 4B, measured by mean fluorescence intensity (VSV-GFP) in HEK293 cells transfected with ISG15 (IRES-mcherry) constructs, relative to the control vector (no ISG15). Data are presented as mean (solid oval) and standard deviation (bars) with individual data points of three biological replicates shown in grey circles.

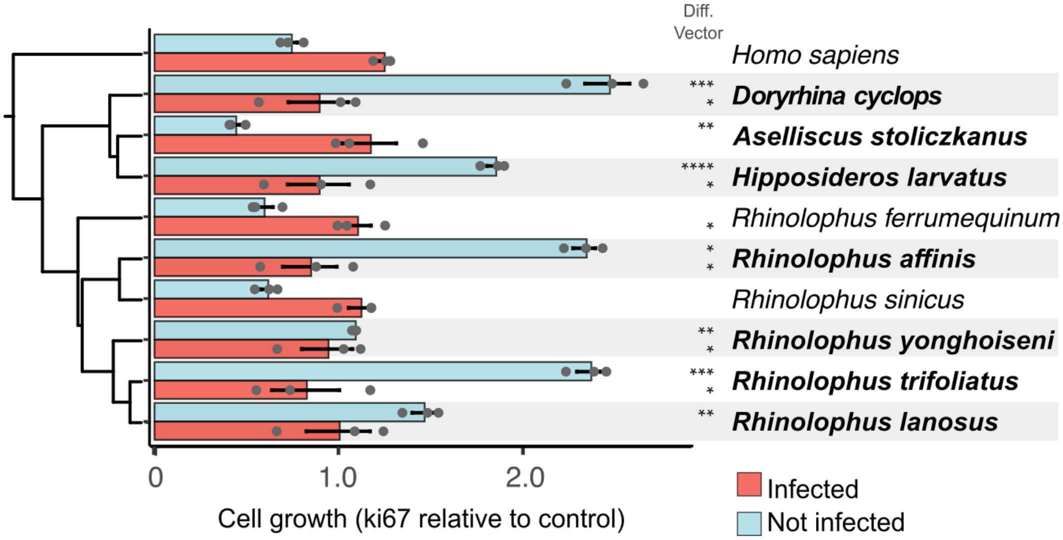

Supplementary Figure 24. ISG15 of some bats affects growth of uninfected HEK293 cells. FACS measurements of Ki-67, a cellular marker for proliferation, in HEK293 cells that were stably transfected with the various ISG15 constructs. Measurements were taken at 16h post-infection and are normalized to the 0h timepoint and the vector control. Thus, values >1 indicate an increase in cell growth compared to the vector control. Three biological replicates are indicated by grey dots and black bars show standard error per treatment.

For uninfected cells, expression of human ISG15 and ISG15 of *A. stoliczkanus*, *R. ferrumequinum* and *R. sinicus* leads to a significant decrease in cell growth, compared to the vector control. In contrast, expression of ISG15 of the six other bats (*D. cyclops, H. larvatus, R. affinis, R. yonghoiseni, R. trifoliatus*, and *R. lanosus*) results in a significantly increased growth of uninfected cells, showing that ISG15 of some bats positively affects cell growth without viral infection. Furthermore, ISG15 of seven bats (exceptions are *R. ferrumequinum* (P=0.08) and *R. sinicus* (P=0.07) induces a significantly different cell growth compared to human ISG15.

For cells infected with GFP-VSV, none of the differences are significant between bat and human ISG15 and only human ISG15 (P=0.0017) results in a significantly different cell growth compared to the vector control.

Significance was tested with a two-tailed t-test compared to the vector control and compared to human ISG15, and is indicated with * P< 0.05, **P< 0.01, ***P< 0.001, ****P< 0.0001. Raw data, means and P-values are provided in Supplementary Table 12.

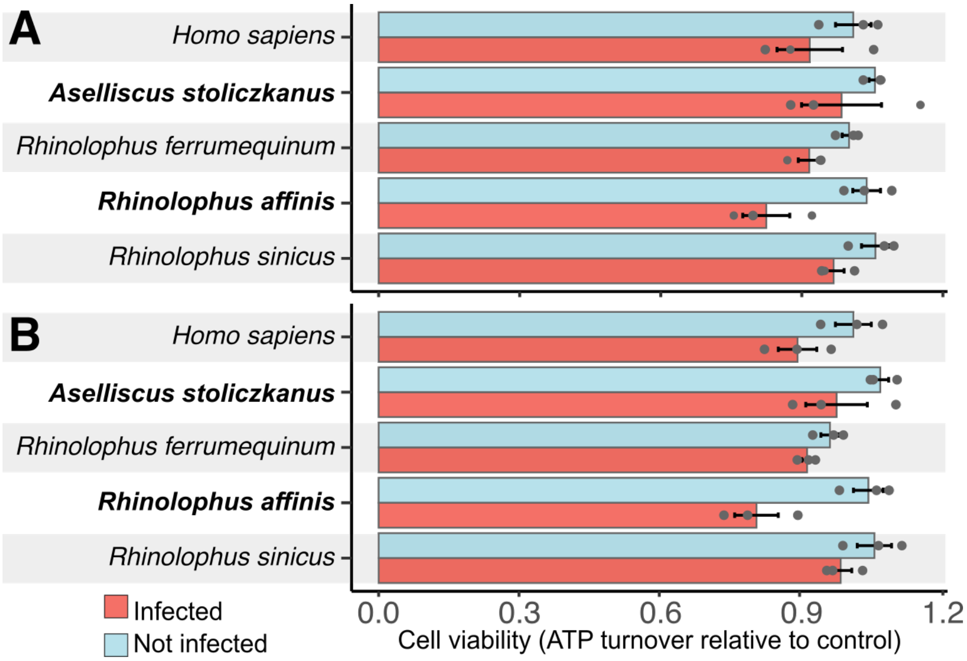

Supplementary Figure 25. ISG15 of some bats affects ATP turnover of uninfected HEK293 cells.

(**A-B**) In addition to cell growth, we also used the CCK8 assay to measure ATP turnover as a proxy for viability of HEK293 cells that were stably transfected with ISG15 constructs. Measurements from 8h (**A**) and 16h (**B**) post-infection are normalized to the 0h timepoint and the vector control. Three biological replicates are indicated by grey dots and black bars show standard error per treatment. For uninfected cells, there is no significant difference for ISG15 of any of the tested species at 8h and 16h compared to the vector control. For cells infected with VSV-GFP, ISG15 of *R. ferrumequinum* and *R. affinis* (but not any other species) significantly reduces ATP turnover compared to the vector control, indicating a cellular response potentially related to modulation of metabolism or protein synthesis (processes known to be affected by ISG15 (Kang, Kim, and Jeon 2022)). There is no significant difference between human and bat ISG15 for infected or uninfected cells.

Significance was tested with a two-tailed t-test compared to the vector control and compared to human ISG15, and is indicated with * $P < 0.05$, **$P < 0.01$, ***$P < 0.001$, ****$P < 0.0001$. Raw data, means and P-values are provided in Supplementary Table 13.

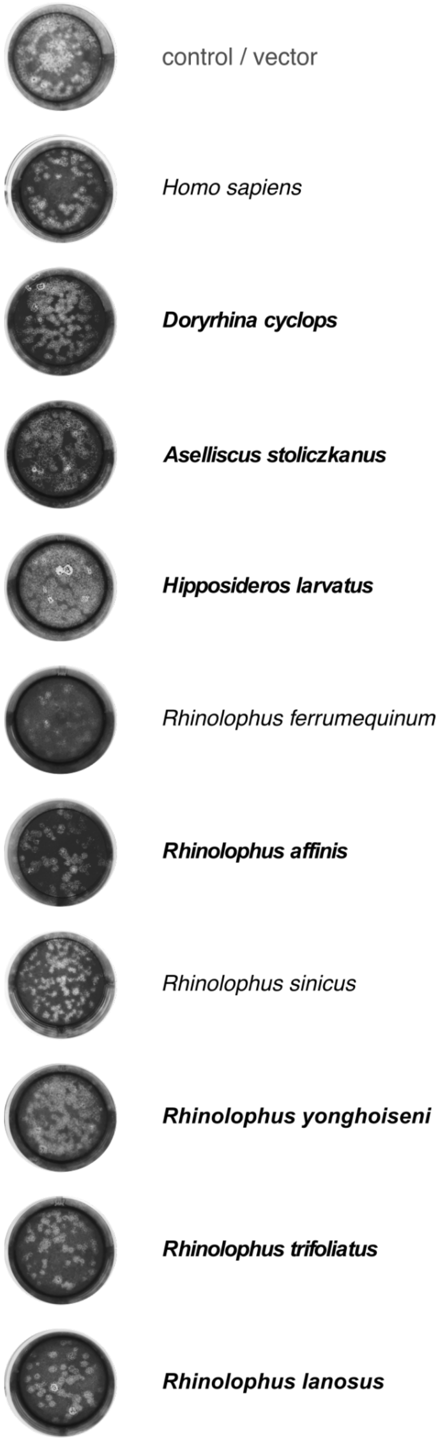

Supplementary Figure 26. IAV plaque assays.
Influenza A virus (IAV) H1N1 plaque assay with stable ISG15-transduced A549 cells infected with virus, direct overlayed with 2% Methyl cellulose for 3 days, fixed and counterstained with 0.1% Crystal Violet in 20% Ethanol. Images of one well representative of three individual experiments are shown as per Figure 4C.

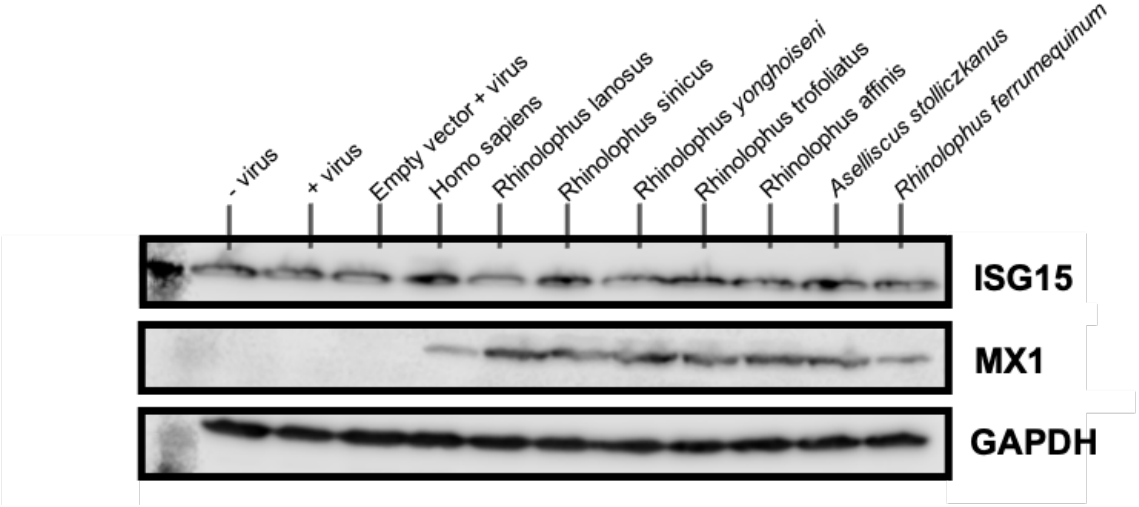

Supplementary Figure 27. MX1 expression in IAV-infected A549 cells expressing ISG15. Western blot of A549 lysate cells transfected with ISG15 and infected with Influenza A virus (IAV) H1N1 for detection of ISG15, MX1 and GAPDH as a control. Data are representative images of three individual experiments (uncropped images shown below). Lysates were collected as previously 48 hrs post-infection. Interestingly, although transfection of *R. sinicus* ISG15 did not result in an obvious antiviral activity against IAV, it resulted in higher MX1 levels, similar to other bats.

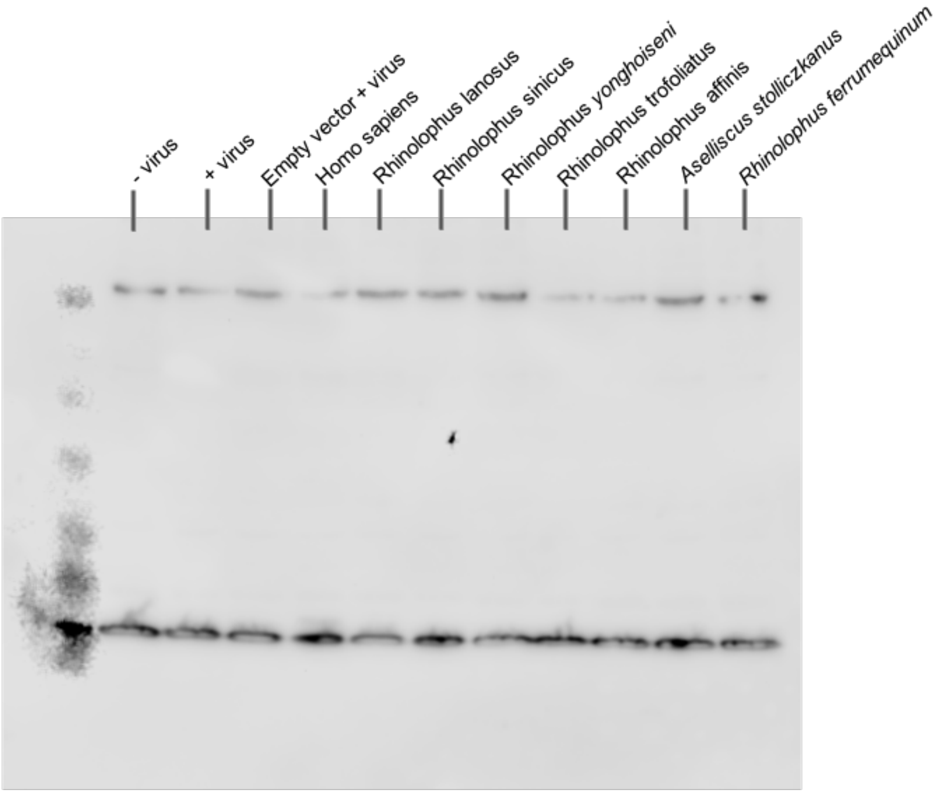

Uncropped Western blot of A549 lysate cells transfected with ISG15 and infected with Influenza A virus (IAV) H1N1 for detection of ISG15.

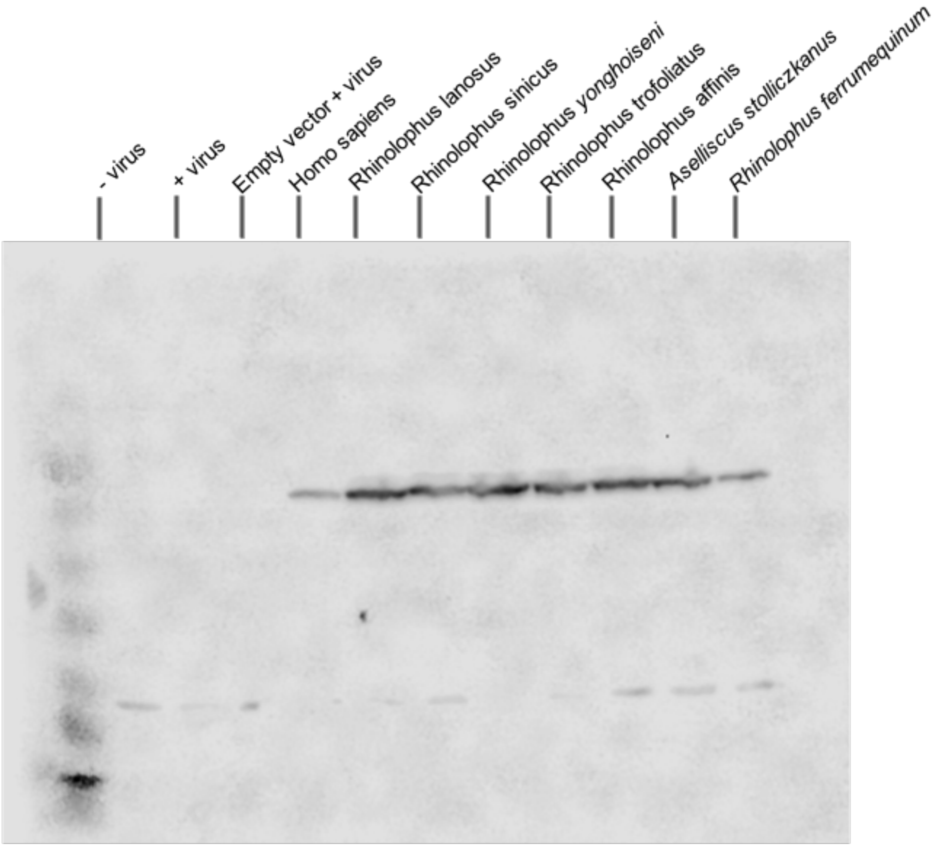

Uncropped Western blot of A549 lysate cells transfected with ISG15 and infected with Influenza A virus (IAV) H1N1 for detection of MX1.

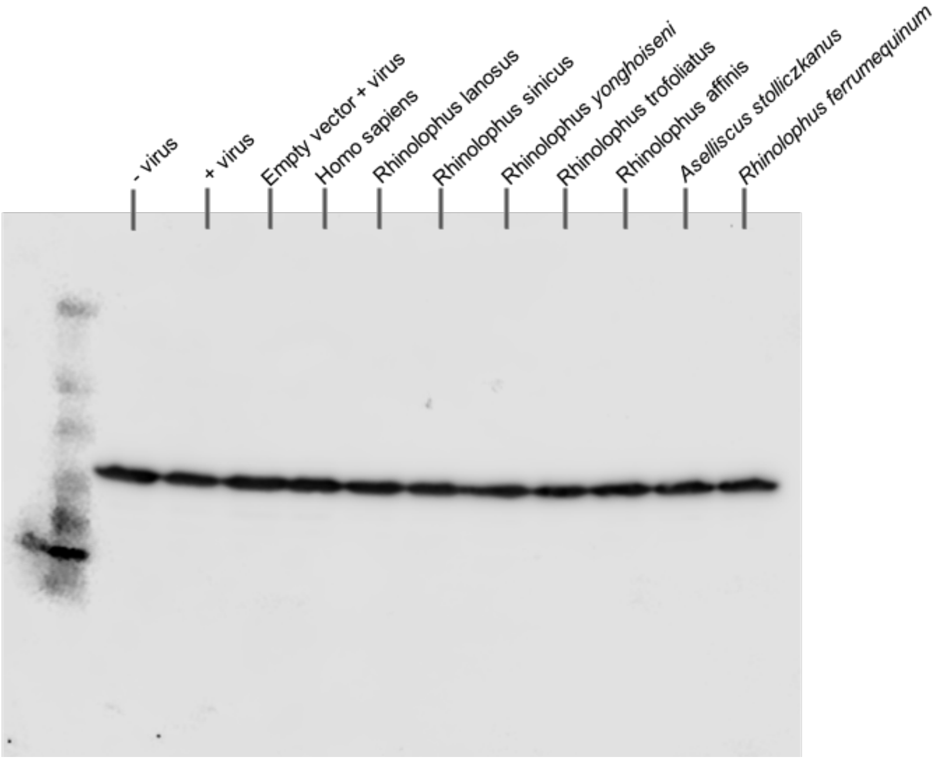

Uncropped Western blot of A549 lysate cells transfected with ISG15 and infected with Influenza A virus (IAV) H1N1 for detection of GAPDH.

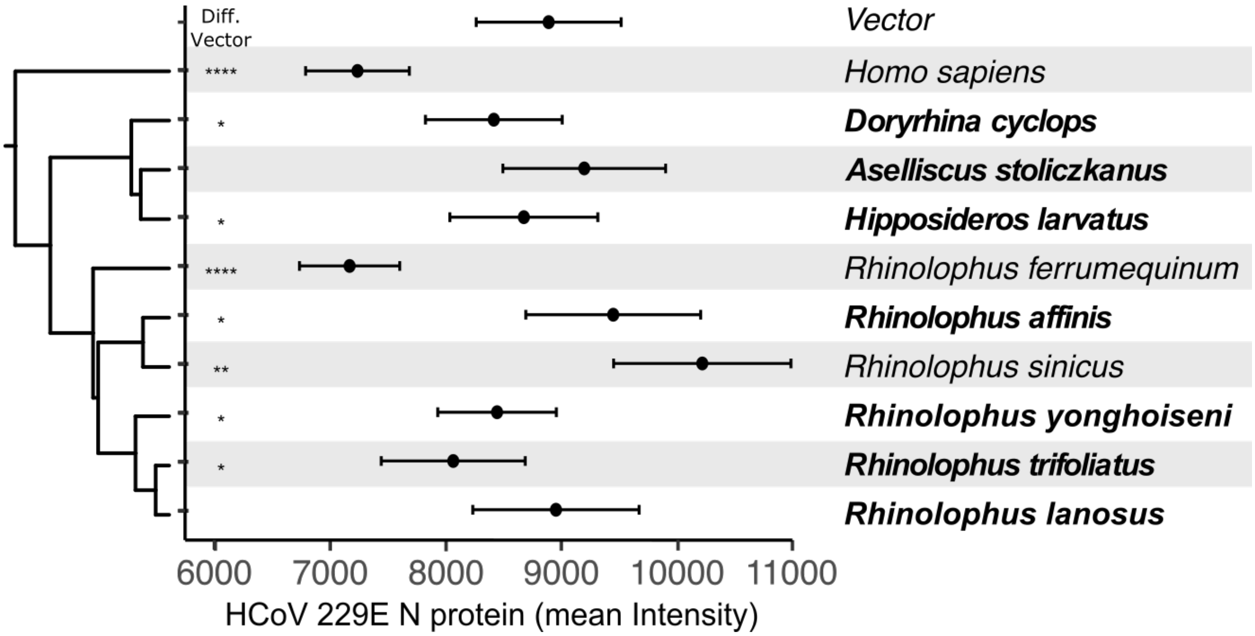

Supplementary Figure 28. Viral load in HCoV-229E HEK293-ANPEP cells with bat-ISG15 constructs.

Viral load as per Fig. 4D, measured by FACS in ISG15-transfected (mCherry positive, IRES reporter) HEK293-ANPEP stable expressing cells infected with Human Coronavirus 229E (HCoV-229E) stained with antibodies for N-protein. Data are represented as geometric mean fluorescent intensities (rlu). Species with newly-sequenced genomes are in bold font. Significant differences to the vector control are indicated with * $P<0.05$, ** $P<0.01$, *** $P<0.001$, **** $P<0.0001$. Significance was determined with a two-tailed t-test. Data are provided in Supplementary Table 16.

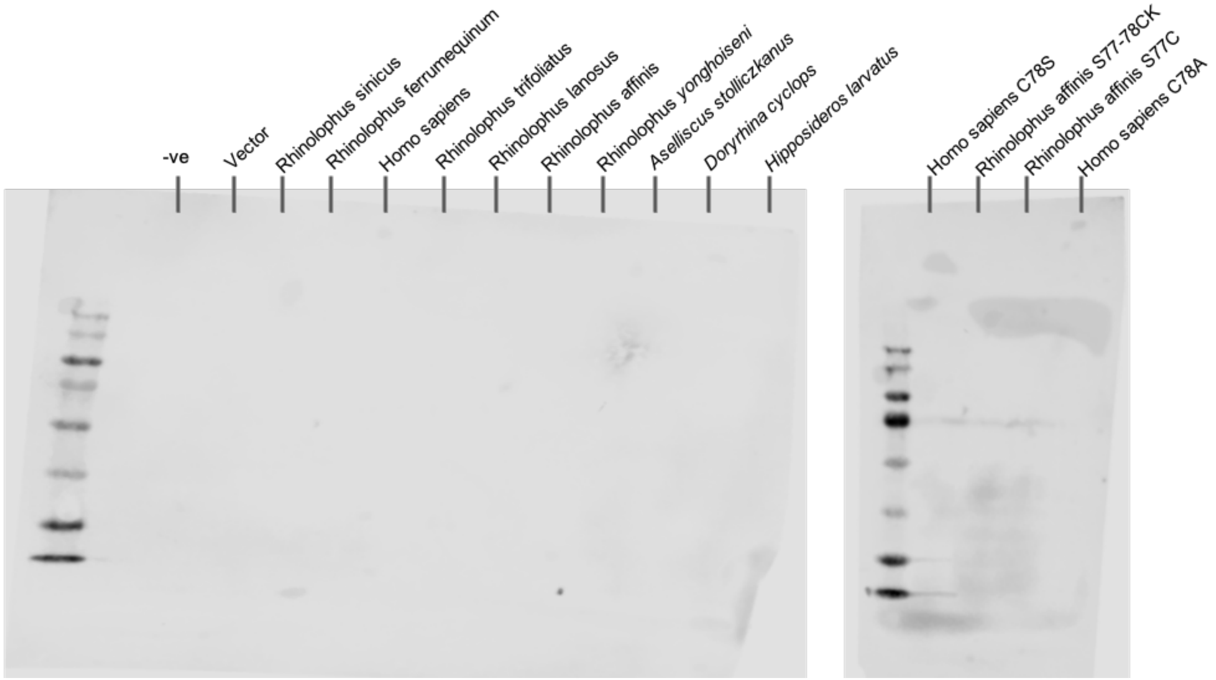

Supplementary Figure 29. Uncropped western blot of cell supernatants of ISG15 transfected HEK293-ANPEP cells without viral infection for detection of ISG15.

Cropped version shown in Fig. 4H. Photos are representative images of three individual experiments.

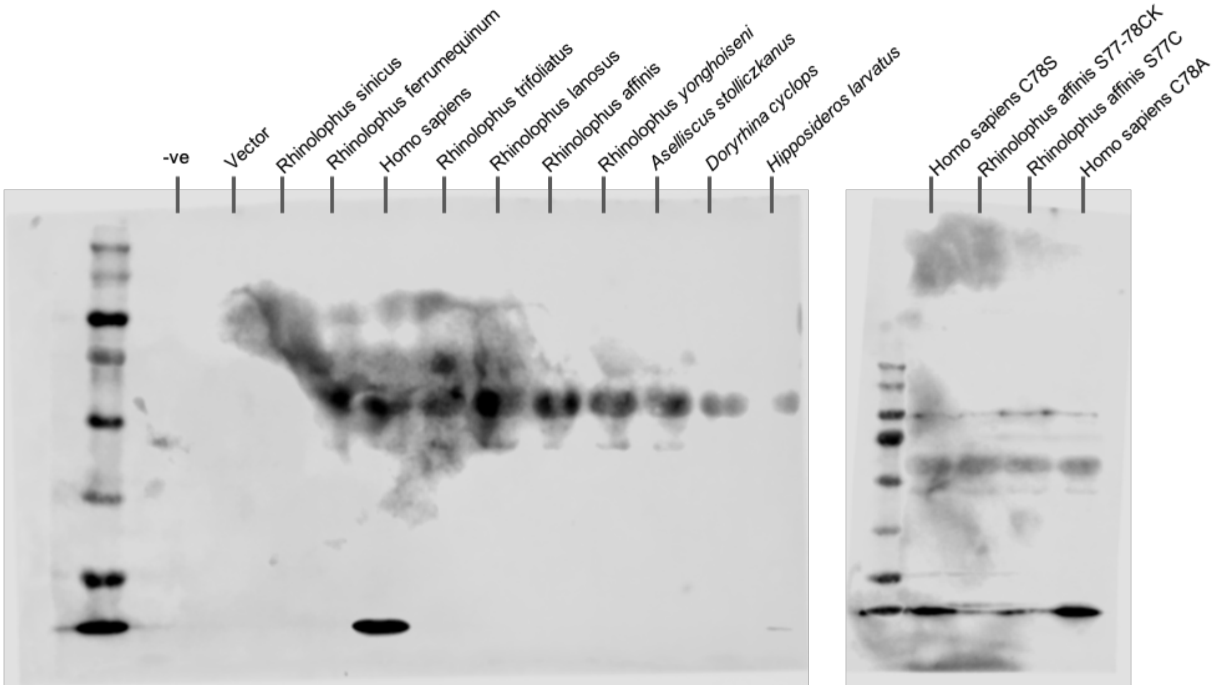

Supplementary Figure 30. Uncropped western blot of cell supernatants of ISG15 transfected HEK293-ANPEP cells after infection with HCoV-229E for detection of ISG15. Cropped version shown in Fig. 4H. Photos are representative images of three individual experiments.

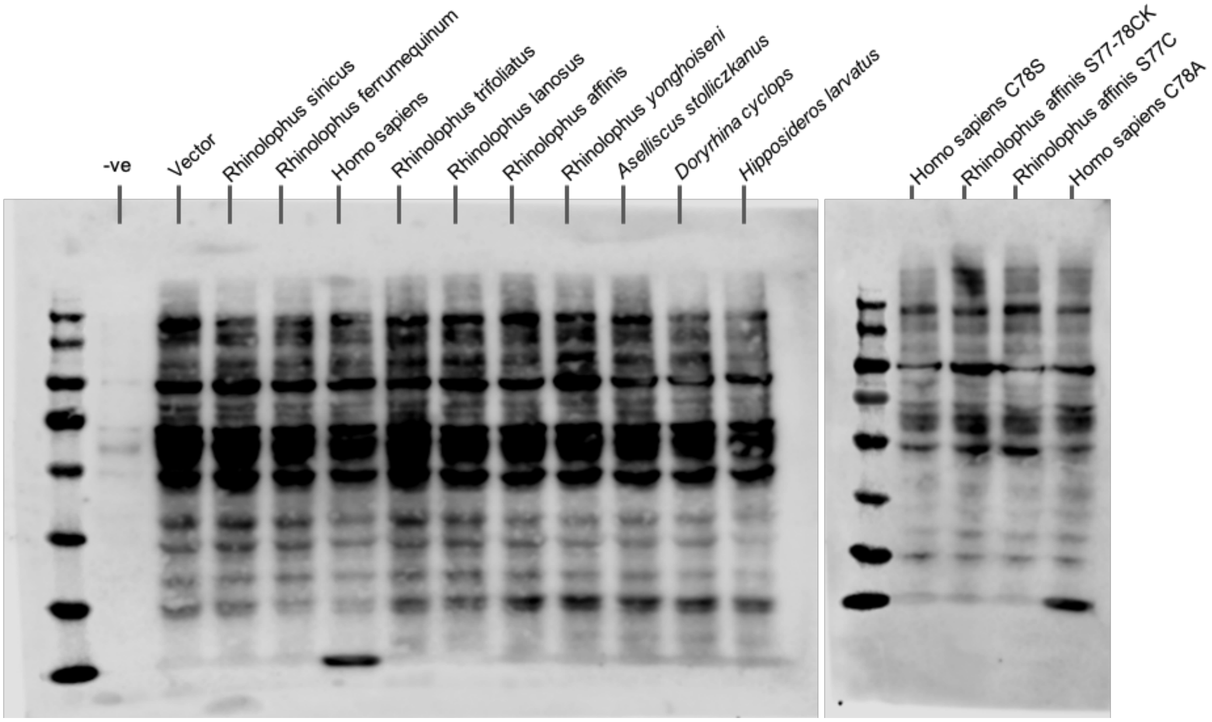

Supplementary Figure 31. Uncropped western blot of cell lysates of ISG15 transfected HEK293-ANPEP cells after infection with HCoV-229E for detection of ISG15.
Cropped version shown in Fig. 4H. The lower band at ~15 kDa represents free ISG15, other bands are ISGylated proteins. HCoV-229E infection induces higher ISGylation levels, even in untransfected cells. Photos are representative images of three individual experiments.

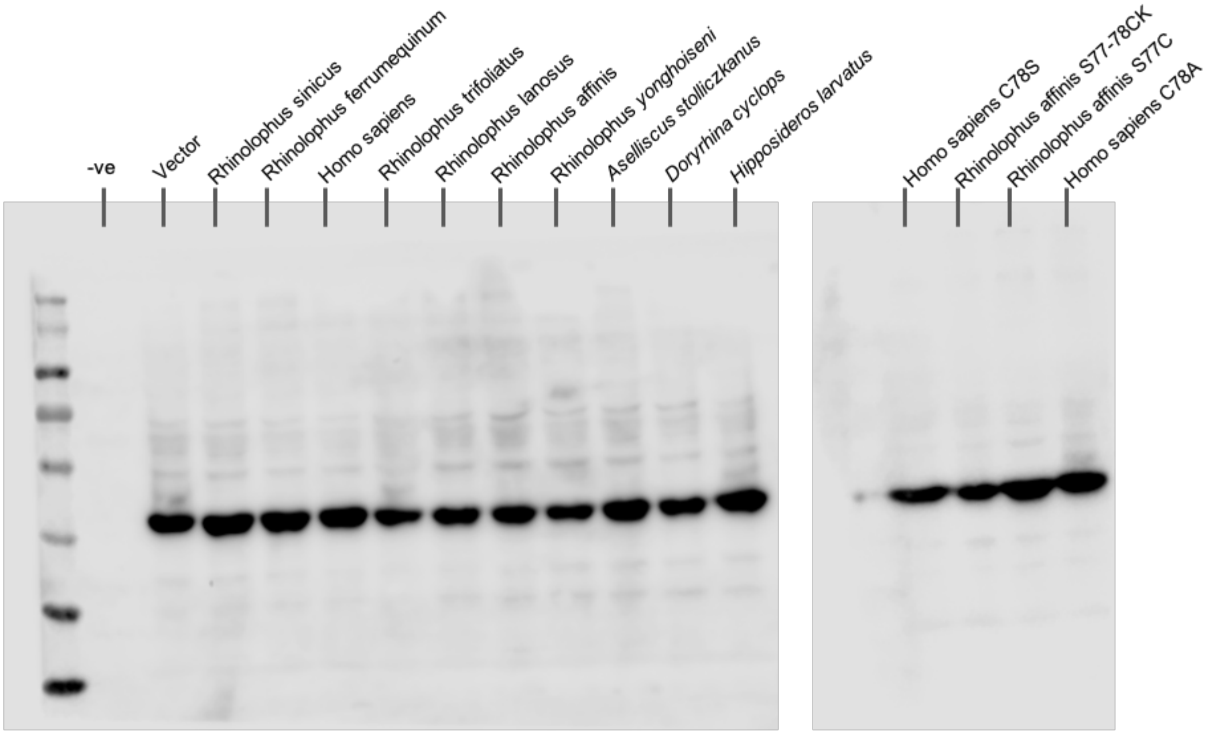

Supplementary Figure 32. Uncropped western blot of cell lysates of ISG15 transfected HEK293-ANPEP cells after infection with HCoV-229E for detection of HCoV-229E N protein. Cropped version shown in Fig. 4H. Photos are representative images of three individual experiments.

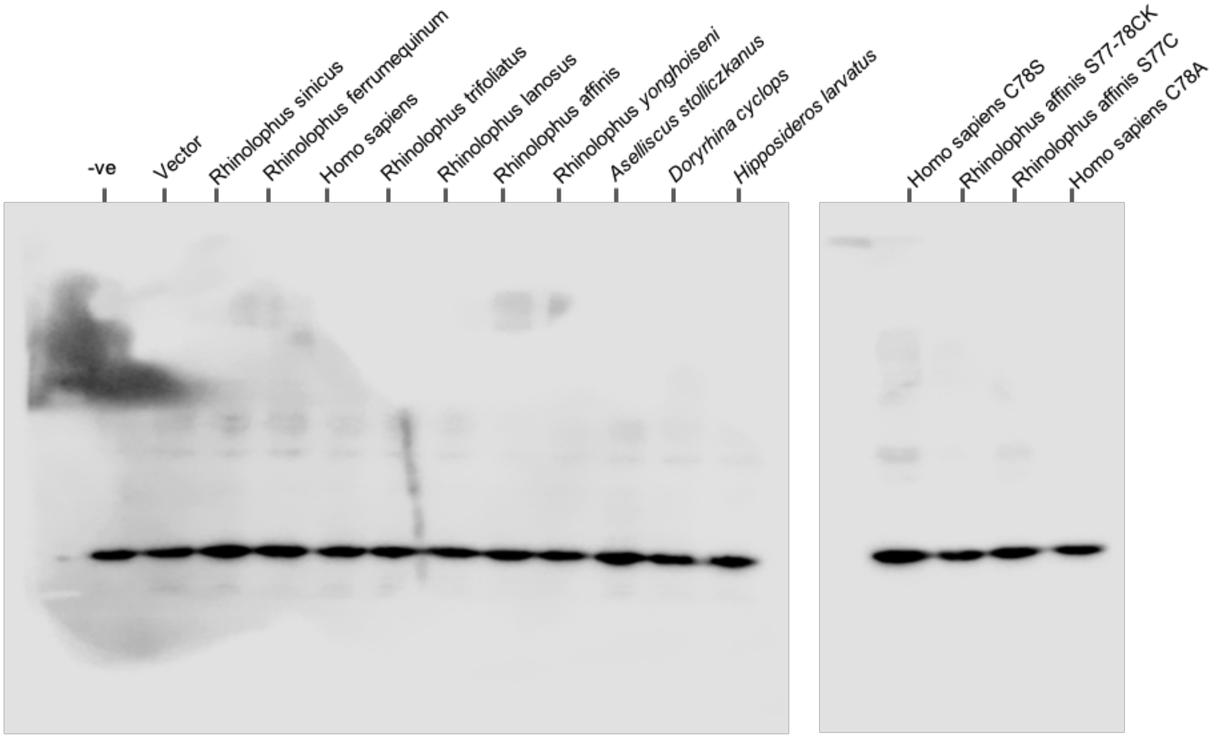

Supplementary Figure 33. Western blot of cell lysates of ISG15 transfected HEK293-ANPEP cells after infection with HCoV-229E for detection of GAPDH (control).

Cropped version shown in Fig. 4H. Photos are representative images of three individual experiments.

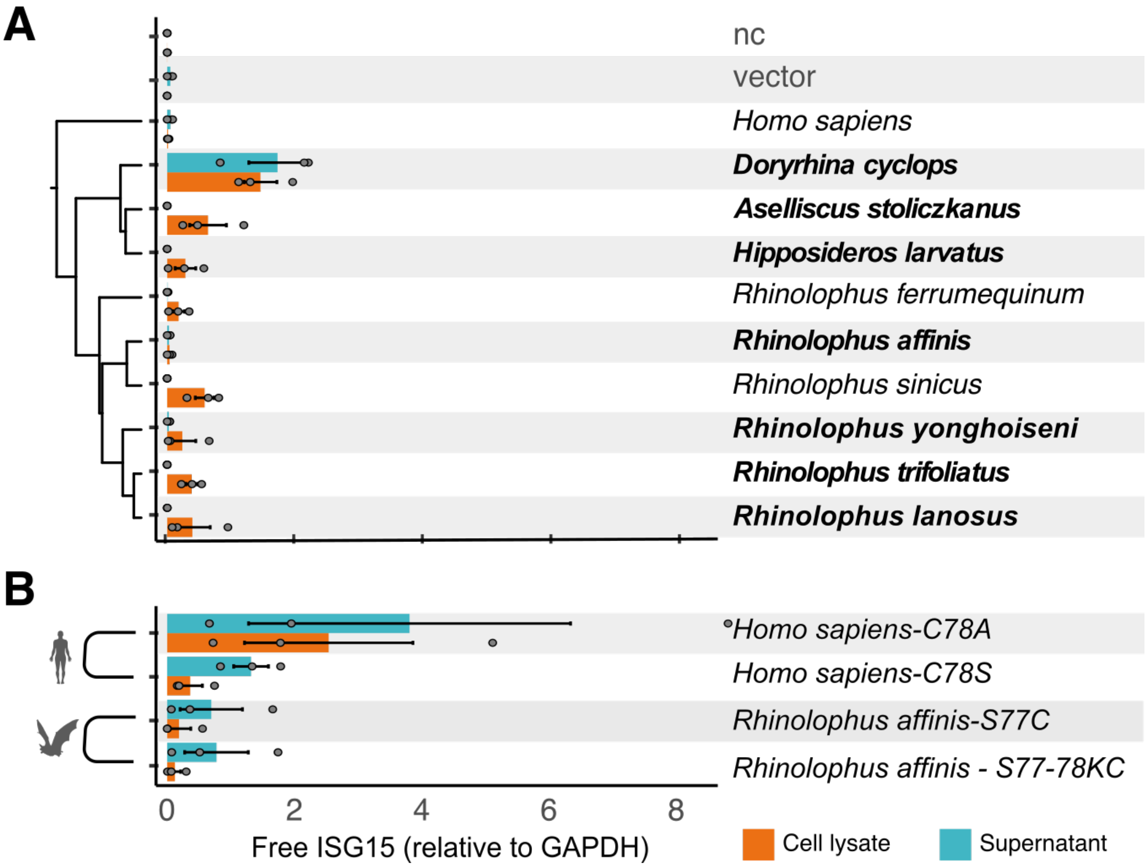

Supplementary Figure 34. Quantification of free ISG15.

Western blot quantifications of cell lysates and supernatants of ISG15 transfected HEK293-ANPEP cells after infection with HCoV-229E for detection of ISG15. We measured mean intensity readings with the FiJI ImageJ software, subtracted the background, and normalized to GAPDH. The graph shows the ratio of ISG15 to GAPDH.

(A) Cells transfected with wildtype ISG15.

(B) Cells transfected with mutant *Homo sapiens* or *Rhinolophus affinis* ISG15 constructs that remove or restore the Cys78 residue.

Three biological replicates are indicated by grey dots and black bars show standard error per treatment. Raw data are provided in Supplementary Table 18.

References

Jebb, David, Zixia Huang, Martin Pippel, Graham M. Hughes, Ksenia Lavrichenko, Paolo Devanna, Sylke Winkler, et al. 2020. “Six Reference-Quality Genomes Reveal Evolution of Bat Adaptations.” *Nature* 583 (7817): 578–84.

Kang, Ji An, Yoon Jung Kim, and Young Joo Jeon. 2022. “The Diverse Repertoire of ISG15: More Intricate than Initially Thought.” *Experimental & Molecular Medicine* 54 (11): 1779–92.

Pettersen, Eric F., Thomas D. Goddard, Conrad C. Huang, Elaine C. Meng, Gregory S. Couch, Tristan I. Croll, John H. Morris, and Thomas E. Ferrin. 2021. “UCSF ChimeraX: Structure Visualization for Researchers, Educators, and Developers.” *Protein Science: A Publication of the Protein Society* 30 (1): 70–82.